Vibration serviceability assessment of the world's longest suspended footbridge in 2020

António Tadeu[a,b,*], António Romero[c], Sara Dias[a], Filipe Pedro[a], Michael Brett[a,d], Miguel Serra[a], Pedro Galvín[c, e], Filipe Bandeira[a]

[a]*Itecons - Institute for Research and Technological Development in Construction, Energy, Environment and Sustainability, Rua Pedro Hispano s/ n., 3030-289 Coimbra, Portugal*

[b]*University of Coimbra, ADAI - LAETA, Department of Civil Engineering, University of Coimbra, Pólo II, Rua Luís Reis Santos, 3030-788 Coimbra, Portugal*

[c]*Escuela Técnica Superior de Ingeniería, Universidad de Sevilla, Camino de los Descubrimientos s/n, ES-41092 Sevilla, Spain*

[d]*University of Coimbra, ADAI - LAETA, Department of Mechanical Engineering, University of Coimbra, Pólo II, Rua Luís Reis Santos, 3030-788 Coimbra, Portugal*

[e]*ENGREEN - Laboratory of Engineering for Energy and Environmental Sustainability, Universidad de Sevilla, Camino de los Descubrimientos s/n, ES-41092 Sevilla, Spain*

* Corresponding author. e-mail: tadeu@itecons.uc.pt

Abstract

This paper investigates the vibrations induced by humans through in situ behaviour tests of the 516 Arouca footbridge (Portugal), the world's longest span in 2020 (516 m). The study consists of in situ experimental tests in which the structure was subjected to wind and pedestrian loads. The bridge is first described, to provide design and construction details, after which its dynamic behaviour is evaluated. The estimated natural frequencies were found to be similar to those previously computed by the finite element method. In addition, modal damping ratios and scaling factors are given. The dynamic responses due to pedestrian loads are then analysed. The

damping ratios were found to increase with higher structural response, which highlights the dependence of the damping ratio on the amplitude of the structural response.

Pedestrian comfort was evaluated by analysing the amplitudes and accelerations of the vibrations and complemented by applying a survey to the visitors. The results of the in situ tests showed that the bridge can provide users with a challenging and rewarding experience as they cross it, without suffering displacements and accelerations that they might find unnerving.

Keywords: suspended footbridge; FE model; in situ testing; experimental analysis; modal identification; pedestrian traffic; human-induced vibrations; human perception; survey.

1- Introduction

With the development of technology, the challenges of construction have been improved, encouraging us to design and construct exceptional structures. Bridges are undoubtedly one of those structures. Slender footbridges have gained popularity over the years, and the structure itself has become a tourist attraction. Constructed in 2020, the 516 Arouca Bridge was at the time of its construction the longest span footbridge in the world. This bridge is in a stunning location within the Arouca Geopark (Portugal), which is recognised as a geological heritage site of international relevance and is classified as a UNESCO Global Geopark. The bridge crosses the Paiva river at height of 175 m in relation to the river bed, linking Alvarenga to Canelas.

When the challenge of designing the bridge was presented to Itecons (bridge design/project authorship), the request was to conceive a structure that would offer an exciting experience, as the location is an attraction for leisure activities and extreme sports such as hiking, climbing, rafting, etc. The level of excitement is related to the height of the bridge in relation to the river bed, its slenderness, and its perceived stability. It is well known that vibration in structures induces a sense of insecurity in people, even though it does not mean that the structure is unsafe. Moreover, it is also well known that people induce vibration in structures [1]–[3].

Large span and slender bridges are more prone to suffer vibration serviceability problems [4], given their usual low stiffness, mass, damping, and natural frequencies. Bridges of this type are often vulnerable to dynamic loads due to the movement of pedestrians. Significant lateral and vertical vibrations are frequently associated with suspension bridges under the movement of pedestrians [5], [6].

There are many guidelines and recommendations relating to this issue [7]–[13]. Despite all the available information, there is no international design code that sets out limits and admissible values for the response of the structure under different actions [11], [14]. The problem of pedestrian-induced vibration is mainly considered in these guidelines/standards in two ways: a) by establishing the range of frequencies that characterise the pedestrian-structure interaction; b) by treating the problem separately in terms of the direction (longitudinal, lateral or vertical) in which the pedestrian action is applied. Most of these standards only establish the need to assess the structure's dynamic behaviour if some of its natural frequencies are within the interaction range and do not define a methodology to check the required comfort level [15].

It is recognised that vibration serviceability criteria are still a matter of ongoing research. Dong et al. [16] used vision-based methods to collect displacement, and velocity to determine serviceability assessment. Rezende et al. [17] developed a methodology to evaluate the dynamic behaviour of long-span steel footbridges based on an equivalent beam model. Nimmen et al. [18] reported a full-scale dataset collected specifically for the further development and validation of models for crowd-induced loading. The pedestrian and bridge motions are registered simultaneously using wireless triaxial accelerometers and video cameras. Venuti and Tubino [19] presented a characterisation of pedestrian-induced loading on footbridges in restricted traffic conditions, and compared the reliability of current guidelines and advanced spectral models in the serviceability assessment of footbridges with respect to vertical vibrations.

The comfort limit ranges according to HiVoSS [13] and SETRA [12] were taken into account in the 516 Arouca design stage, meaning that it was ensured that the first natural frequencies occur below the critical range frequencies and the dynamic behaviour under pedestrian excitation was evaluated. The acceleration related indices combined with vibration frequencies were used to define the serviceability limit.

In two previous studies [20], [21], the authors analysed the wind load effects on the 516 Arouca Bridge and presented a design approach to analyse the quasi-static and dynamic behaviour of the bridge through theoretical, analytical, and numerical models. The uncertainties, when it comes to defining the structural and loading parameters in the serviceability assessment of footbridges, led to an in situ experimental work that validated the assumptions made during the design phase [22], [23].

In fact, it is crucial to ensure in the design phase that a structure will provide enough comfort to the users, since vibration problems can be difficult and very expensive to solve after construction. Very recently, and probably due to this new tendency for big span bridges, several studies [16], [24]–[28] have focused on investigating the vibration serviceability of footbridges. For instance, Cao and Chen [29] proposed an online big data approach to investigate the limits of vibration serviceability in a real environment. A smartphone-based application was developed to assess data on personal judgment of vibration level, vibration signals, environmental, and biological factors. That kind of information is needed, gathering data on the human perception of the structural dynamic response. With this in mind, a survey is being given to tourists on the 516 Arouca Bridge so that we can acquire this kind of data. The present study considered the answers of 1030 visitors (data available so far) about the experience.

This paper pursues already ongoing experimental work by studying the vibrations and displacements induced by the wind and by pedestrians through in situ behaviour tests on the 516 Arouca. Bridge responses caused by people walking at different speeds, running, jumping,

and swinging (simulating a deliberately harmful action) as they crossed it were recorded. All tests were performed under similar very low wind conditions.

The next section presents relevant information about the design codes and guidelines on this subject. The 516 Arouca bridge is described in Section 3. Section 4 briefly presents the finite element (FE) model used in the bridge design and reports the HiVoSS and SETRA approach used to determine the maximum acceleration through FE models. Details of the in situ tests are given in Section 5. Then, the modal parameters, including the damping ratios, of the structure are identified from an operational modal analysis (OMA) in Section 6. In addition, the dynamic behaviour of the bridge is analysed from different pedestrian loads and deliberately harmful - vandal - loading. The last section assesses the comfort classes of the bridge according to the European guidelines HiVoSS and SETRA and by presenting the inquiry results. The results are presented and discussed, and conclusions are drawn.

2- Design codes and guidelines

The first design code that involves vibration serviceability is BS 5400-2 [4]. It presents a procedure to check for vertical vibrations caused by a single pedestrian and was defined for footbridges whose natural frequency of the fundamental vertical mode of vibration was up to 5 Hz. The Ontario Highway Bridge Design Code [14] requires the determination of the dynamic response of a bridge to a simulated footfall force, analogous to BS 5400-2[4]. Many years later, in 2002, the code was updated to the version that is still in force, BS 5400: BD 37/01 [15]. The main modification to the code was the requirement to also check vibration serviceability in the lateral direction. This additional requirement derives in part from experience with lateral vibrations of the London Millennium Bridge [13]. Pedestrians are more sensitive to horizontal vibrations than to vertical ones, and vibrations are higher in crowded conditions. For this reason,

lower limit values for lateral vibrations were established. All footbridges with fundamental lateral frequencies lower than 1.5 Hz now have to undergo a dynamic analysis.

SETRA and HiVoSS are currently the more complete and widely used guidelines to design this type of bridge [16]. Even though these codes recommend vibration comfort limits, they also state that it is up to the building promotor/builder to decide which comfort limits are to be met. The methodology provided by these guidelines classifies the footbridge in terms of the required comfort level and the expected level of traffic. However, this classification cannot be considered an absolute criterion because the concept of comfort is highly subjective and the acceleration feeling is experienced differently. To take this subjectivity into account, the guidelines establish ranges rather than thresholds. In fact, both guidelines provide the same four ranges of accelerations, distinguishing between vertical and lateral: maximum, mean minimum, and uncomfortable/unacceptable.

However, the comfort limit ranges according to HiVoSS [13] and SETRA [12] were taken into account in the design stage, thereby ensuring that the first natural frequencies occur below the critical range frequencies and confirming the need for a dynamic evaluation of pedestrian excitation. These guidelines are only used to assess vibration comfort limits when a group of people walk on the bridge. Figures 1 and 2 illustrate the limits of both the critical ranges for natural frequencies with pedestrian excitation, and the defined comfort classes with common acceleration ranges, respectively.

Regarding the critical range of frequencies, SETRA defines four classes, while HiVoSS only distinguishes acceptable from critical (two classes). In the HiVoSS guideline, it is considered that the lateral vibrations are not affected by the second harmonic of pedestrian loads. However, it considers that the bridge might be excited to resonance by the second harmonic of pedestrian loads for vertical accelerations in bridge structures with natural frequencies between 2.5 Hz and

4.6 Hz. In that case, the critical frequency range for vertical and longitudinal vibrations expands to a larger range [1.25 to 4.6] Hz.

The two guidelines define identical comfort classes regarding acceleration values (Figure 2). Both also alert to the lock-in phenomenon, which can be triggered by lateral acceleration levels exceeding 0.1 m/s^2.

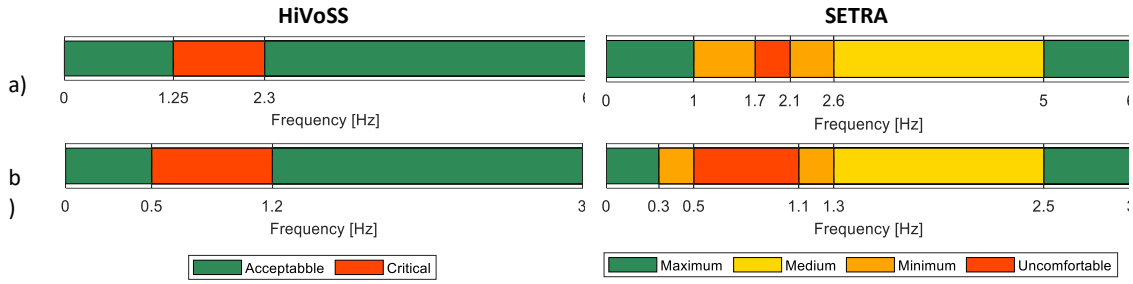

Figure 1: Frequency comfort limit ranges according to the European guidelines HiVoSS and SETRA: a) Vertical direction; b) Lateral direction.

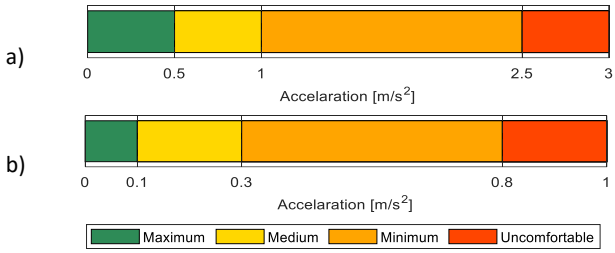

Figure 2: Acceleration comfort limit ranges according to the European guidelines HiVoSS and SETRA: a) Vertical direction; b) Lateral direction.

3- The Arouca 516 footbridge

The structure under study is a suspension bridge for pedestrian use, with a span of 516.5 m. The suspension system consists of two main cables (catenaries) and hangers (main and secondary), which support a total of 127 metal deck modules. Each catenary is composed of seven steel wire ropes (steel core, E=100GPa, *m*=51kg/m and A=5915 mm^2), with a wire rope nominal diameter of 40 mm. The ends of these cables were attached to the anchoring blocks, and the cables were placed resting on a saddle at the top of the pillars, 36.3 m high. The main cables are 530.305 m long with a sag of about 53.56 m.

The hangers are composed of a single wire rope with a nominal diameter of 12 mm. The hangers vary in length between 2.361 m and 35.684 m. A single deck module is 4016 mm long and 2100 mm wide. It is made mainly from UPN profiles and some angle profiles, all of S275 steel. The floor of the module is made of a lightweight steel grid panel.

The modules are connected through nodes fitted at the ends, where the hangers are also connected. Each module (with a mass of 505.6 kg) is hung from the catenaries via a total of 8 secondary cables, which are shared with the adjoining modules. Of these eight cable hangers, 4 are designed to carry most of the gravity load (main hangers) and the other 4 are post-tensioned secondary hangers designed to reduce the rotation of the deck and prevent some lateral movement.

a)

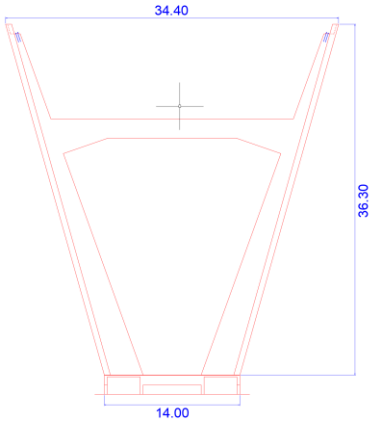

b)

c)

d)

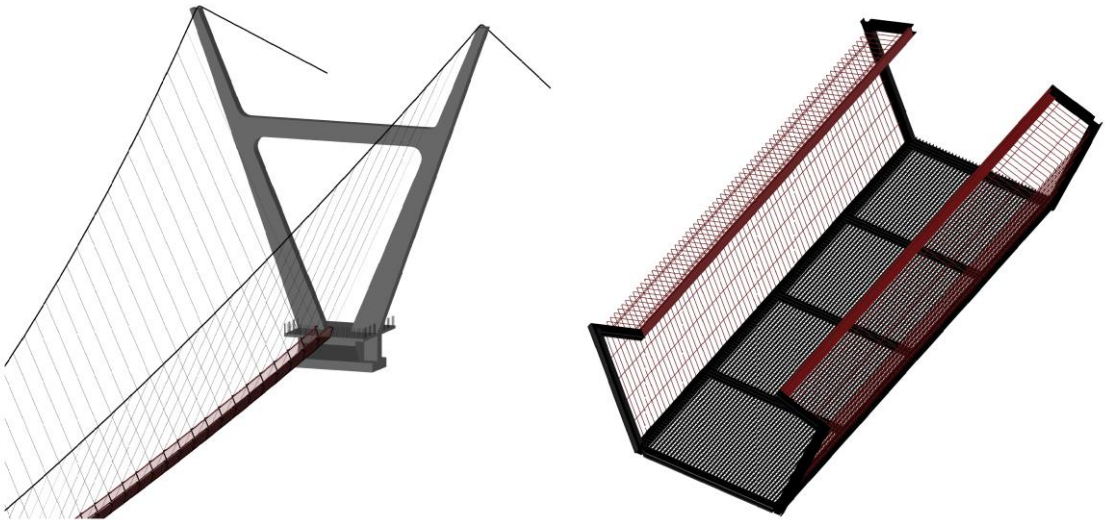

e) f)

Figure 3: Views of the Arouca 516 Bridge: a) View from the Alvarenga side; b) Bridge pillar design (dimensions in m); c) Generic view; d) View from underneath; e) Structural design of the bridge; f) Structural design of the module with the deck and lateral grids.

4- Finite Element simulation of the bridge

Simplified theoretical, analytical and numerical models were used in a preliminary design stage to define the bridge configuration under static and dynamic loading to ensure [21]:

6) a relatively low tensile force on the main cables when struck by wind up to a velocity of about 190 km/h and a live load of 2.2 kN/m^2;

ii) low inclination of the deck modules in the longitudinal direction (less than 15%);

iii) low displacements on the bridge when a group of 34 people cross the bridge (less than 1.5 m);

iv) natural frequencies of the first eigenmodes below the critical ranges indicated by the European guidelines HiVoSS and SETRA associated with pedestrian excitation (0.5 Hz

for lateral vibrations and 1.25 Hz for vertical and longitudinal vibrations, the lower limits of the critical ranges);

v) maximum admissible vertical accelerations using harmonic load models defined according to the number of pedestrians on the bridge (less than 1.75 m/s^2).

In the present work, a numerical finite element model (FEM) was created using Autodesk® Robot Structural Analysis Professional software [30]. Its capabilities were explored to model cable structures subjected to large displacements, to define initial stress conditions, and to execute a modal analysis considering a stress state at the end of a static analysis.

The cables were modelled using cable elements (tension only, 6DOF), whereas the elements forming the deck were modelled considering 12DOF Euler-Bernoulli beam elements (see Figure 4). Three nodes were added at the end of each deck module, defined by *L*, *C,* and *R*, where the load was applied. These correspond to the theoretical concentric and eccentric centre of mass loads of human bodies, coupled with the centre of mass of the deck (see Figure 4). All loads were applied to the previously mentioned locations. Loads due to self-weight and wind action were modelled as a concentrated load at point *C*, while those arising from human activity were modelled at any of the 3 points, depending on the case under study. The masses used in the modal analysis are equally modelled at these 3 points, with the same assumptions.

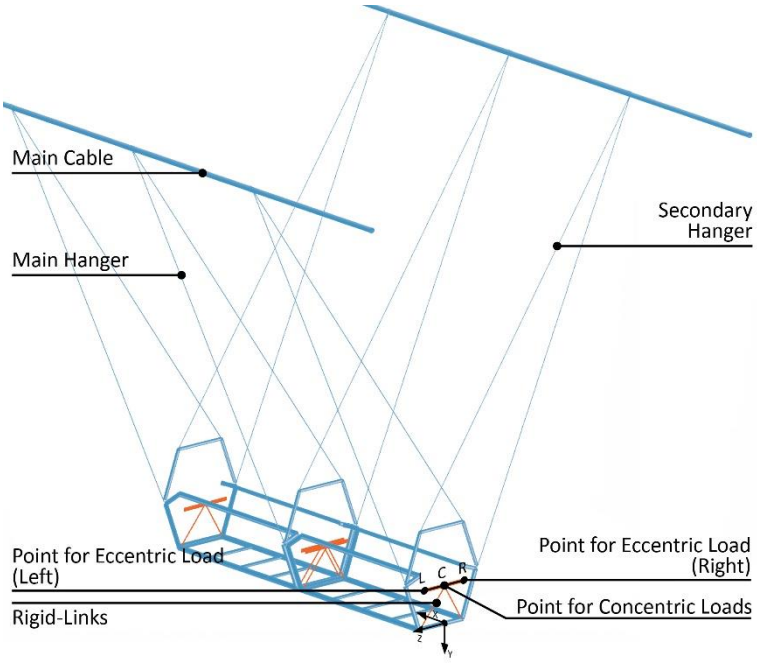

Figure 4: Sectioned view of the numerical model.

The model of the bridge was initially used to evaluate the natural frequencies and associated modes. This was accomplished in two stages: 1) a nonlinear analysis was performed to determine the shape under self-weight and the corresponding stress state of the structure; 2) a modal analysis was carried out to determine the modal properties of the bridge using the stress state obtained at the end of stage 1. Static and dynamic studies were performed using large displacement geometrically nonlinear analysis and applying a full Newton-Raphson solver, as required for a good estimation of the structure's geometric stiffness. This analysis saves the total stiffness and mass matrices at the end of the iterative process. This results in a stiffness matrix, also called a secant stiffness matrix, which is used as an input for the modal analysis and takes into account the extra geometric stiffness that arises from tensioned elements.

After defining the modal parameters, the maximum acceleration provided by uniformly and non-uniformly distributed loads $p(t)$ was computed for different numbers of pedestrians and different structural damping ratios according to the European guidelines HiVoSS and SETRA,

$$p(t) = P\,cos\left(2\pi f_s t\right)n'\psi \qquad (1)$$

where P is the component of the force due to a single pedestrian (280 N for vertical, 140 N for longitudinal, and 35N for lateral vibrations) with a walking step frequency f_s, which is assumed to be equal to the footbridge natural frequency computed using the FEM model for the vertical or lateral directions. $n' = \frac{10.8\sqrt{\xi n}}{s}$ (for a density lower than 1.0 pedestrian by square meter) is the equivalent number of pedestrians on the loaded surface where n is the number of the pedestrians on the loaded surface. The parameter ψ is the reduction coefficient defined differently according to HiVoSS and SETRA guidelines (see Figure 5), following the comfort frequency limit ranges given in Figures 1 and 2. In the case of the SETRA guideline, the second harmonic is only considered for a density greater than 0.8 pedestrians by square meter. The sign of $p(t)$ is assumed to vary according to the mode shape to maximize the vibration of the bridge. This load must therefore be the same as the direction of the mode shape, and must be inverted each time the mode shape changes direction. These loads are applied until the maximum acceleration of the resonance is reached, ascertained by evaluating the time history analyses. In these calculations, each individual pedestrian's mass is incorporated within the footbridge's mass.

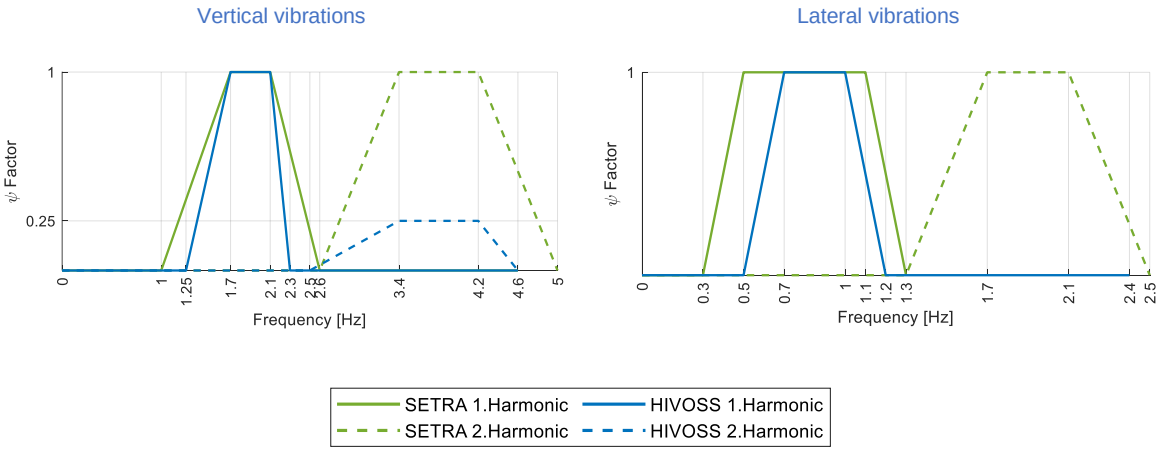

Figure 5: Factor ψ for the vertical and lateral vibrations according to HiVoSS and SETRA guidelines.

5- In situ tests

In November 2020, a series of experiments were carried out on the 516 Arouca bridge to characterise its structure by investigating the vibrations and displacements induced by the wind and by pedestrians through in situ tests. The experimental set-up, the group description, and the tests are described next.

5.1 Experimental set-up

The bridge response was measured by a set of instruments summarised in Table 1.

Table 1: Equipment used to monitor the bridge.

Equipment	Manufacture and Model	Number	Position
Seismometer [31]	SYSCOM MR3000C (precision timing system clock < 1 ppm; nominal sensitivity of 1.25 V/g; frequency range from DC to 600 Hz; internal clocks were synchronised)	10	Nine seismometers were installed on the upstream side of the platform, along the span of the bridge at the positions indicated in Figure 6 (1/6, 1/4, 1/3, 5/12, 1/2, 7/12, 2/3, 3/4 and 5/6 of the span). Another seismometer was placed at the midspan on the downstream side of the platform.
GNSS Antennas [32]	Leica model GS15 (acquisition rate of 20 Hz and an accuracy of 3 mm (RMS))	3	The GNSS antennas were placed at positions 1/2, 2/3, and 3/4 along the bridge span.
Anemometer [33]	Gill windsonic 2D	1	The anemometer was placed at the bridge midspan.

All items of equipment were fixed to the deck module so that their bases remained horizontal, with the x-axis aligned with the longitudinal, the y-axis pointing vertically, and the z-axis pointing downstream in the lateral direction.

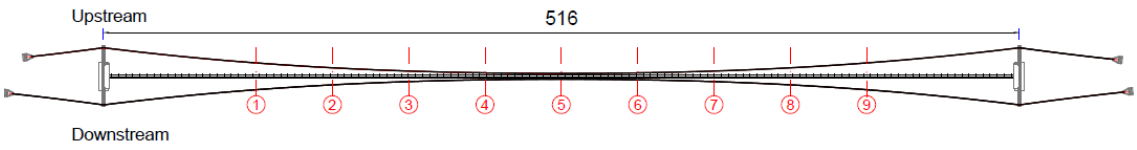

Figure 6: Location of the sensors along the span of the bridge.

5.2 Group description

A group of 34 volunteers, which is equivalent to a total mass of approximately 2778 kg, was invited to participate in this study. The average characteristics (with standard deviations) were

as follows: 42.71±13.94 years of age, a weight of 81.17±11.36 kg, and a height of 1.73±0.09 m. 74% were male, and 26% were female. Thirty-four is the maximum number of people expected to be allowed to cross the bridge simultaneously, as part of a guided tour. The acceleration responses were recorded when the bridge was subjected to the loading caused by people walking at different speeds, running, jumping, and swinging (simulating a deliberately harmful action).

5.3 Tests protocol

Nine different tests, repeated at least twice, were performed on the footbridge to simulate various types of usage. The wind effect on the bridge without anyone on it was recorded for a period of half an hour. The A/D conversion was carried out at a sampling frequency, fs = 200 Hz, which avoided aliasing effects. The structural responses were filtered by applying a 50 Hz Bessel low pass filter of the 8th order to limit the analysis in the frequency range of interest 0-20 Hz [13]. These tests are summarised in Table 2.

Table 2: Tests carried out on the footbridge to simulate different types of pedestrian-induced vibrations and the wind effect.

Actions	Test	Description
Walking	1	A group of 34 people crossed the bridge at a speed of 0.5 m/s.
	2	A group of 34 people crossed the bridge at a speed of 1.0 m/s.
	3	A group of 34 people crossed the bridge at a speed of 1.5 m/s.
	4	A group of 34 people crossed the bridge at random pace and without synchronisation of the steps.
Running	5	A group of 34 people crossed the bridge at a speed of 2.5 m/s.
Jumping	6	People were placed symmetrically around the module located at position 1/4 of the span bridge, and jumped simultaneously.
	7	People were placed symmetrically around the module located at position 1/3 of the span bridge, and jumped simultaneously.

Swinging the structure of the bridge transversally	8	A group of 34 people were placed symmetrically around the platform module position 1/3 of the bridge and asked to move simultaneously to provoke the movement from the upstream to the downstream side and thus induce a swinging movement of the bridge.
	9	Two groups of 17 people were symmetrically arranged around modules at positions 1/3 and 2/3 of the bridge. These groups were asked to provoke the movement of the bridge in a coordinated way, from the upstream side to the downstream side of the modules, thus causing the bridge to swing (symmetric and antisymmetric to the longitudinal axis of the bridge).
Wind action	10	Wind was the only dynamic load applied to the bridge.

For all tests, people were distributed randomly over the platform deck modules. The prevailing health regulations imposed under the COVID-19 pandemic meant that the volunteers were spaced from each other to ensure a maximum of 3 people per deck module. So, the group was distributed over a set of 12 adjoining deck modules. The pace set by the group was controlled by two people, one with a digital metronome at the head of the line and another at the end, ensuring that pace synchronisation was sustained during the bridge crossing. The two metronomes were synchronised with one another using an internal system that set a starting time using a wireless network. The wind velocity and direction recorded by the anemometer were analysed to define the test weather condition. The purpose of the wind monitoring was to ensure that it didn't have a significant impact on the bridge vibrations compared to the pedestrians and that it could be treated as noise. Figure 7 illustrates the wind velocity registered during the first test, in which the wind speed was in the range of 1.5 – 3.0 m/s for 79% of the registered data. The wind velocity and direction distribution of Test 1 was considered representative for all tests. The bridge has an approximate east-west orientation. Thus, the wind direction is almost normal to the bridge. The vibration of the bridge without pedestrians, (only subjected to the wind action), was used to evaluate the bridge's natural vibrations and mode shapes.

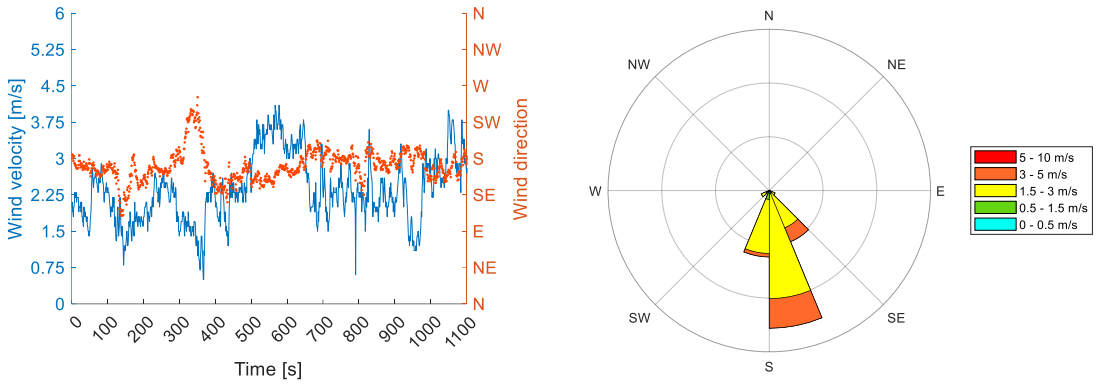

Figure 7: Wind velocity and direction (test 1).

6- Evaluation of the dynamic behaviour of the footbridge

6.1 Modal parameter identification

Natural frequencies and modal damping ratios were identified from the structural response due to wind action (Test 10) acquired over 1800 s per channel. The data were sampled to 200 Hz. The structural response was filtered by applying a 30 Hz Chebyschev low pass filter of the 8th order to limit the analysis in the frequency range of interest 0-6 Hz. The modal parameters were found from an operational modal analysis (OMA) using enhanced frequency domain decomposition (EFDD) [34]. The EFDD technique is based on the decomposition of the power spectral density matrix using the singular value decomposition (SVD).

Figure 9 represents the SVD of the acceleration caused by the wind action using four projection channels and a frequency resolution of 0.0097 Hz. The range of frequencies analysed (from 0 – 6.0Hz) has been defined to assess the risk of resonance entailed by pedestrian traffic according to HiVoSS and SETRA guidelines. The peaks found in the curves correspond to the natural frequencies of the structure. Some peaks related to in-plane mode shapes are found in the comfort limit ranges given in Figures 1 and 2. The HiVoSS and SETRA guidelines state that pedestrian bridges with natural frequencies in these ranges should be subjected to a dynamic evaluation of pedestrian excitation, which is the aim of this section.

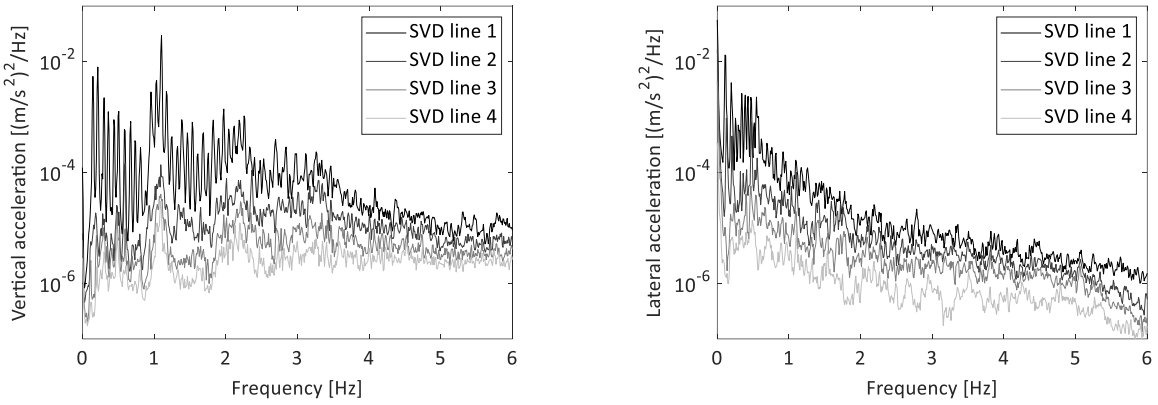

(a) (b)

Figure 8: Singular Value Decomposition from ambient vibration (wind action, test 10) for (a) in-plane and (b) out-plane mode shapes.

The experimental mode shapes are initially estimated as unit norm vectors from the OMA. They are then scaled using the mass-normalised mode shapes of the finite element model described in Section 4. The experimental mass normalised mode shapes are found by the least squares solution of the following [35]–[37]:

$$\{\psi_{Exp}\}_j = [\phi_{FE}]\{R\}_j \quad (2)$$

where, $[\phi_{FE}]$ is a matrix that collects the FE mass normalised mode shapes and $\{R\}_j$ is a transformation vector. Then, the experimental modal mass is estimated as [35]–[37]:

$$m_{Exp,j=}\{R\}_j^T\{R\}_j \quad (3)$$

and the related j-the scaling factor is obtained as $\alpha_j = 1/\sqrt{m_{Exp,j}}$. Then, the identified experimental mode shapes are mass normalised, and the modal kinetic energy is proportional to m_{Exp}.

As mentioned before, The FE model was first used to obtain the natural frequencies and mode shapes. Figures 9 and 10 illustrate the first out-of-plane (lateral displacement) and in-plane modes (vertical displacements).

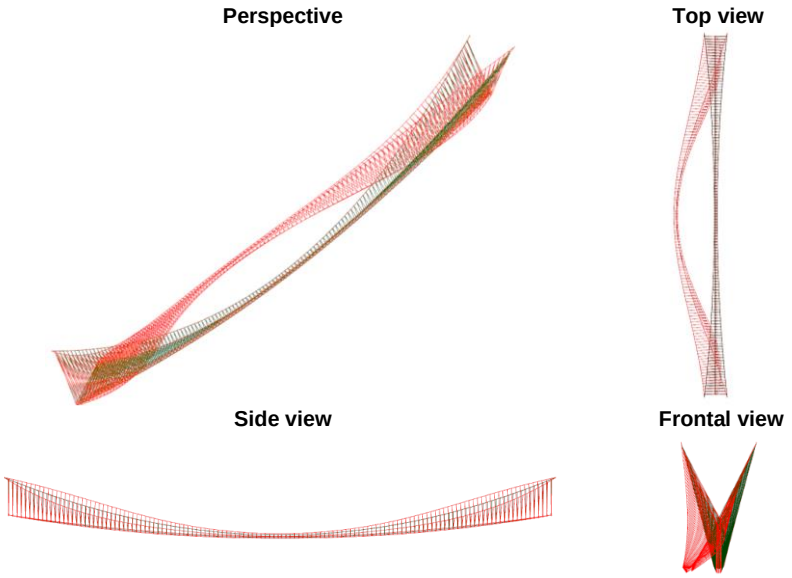

Figure 9: First out-of-plane mode shapes obtained numerically be the FE model (frequency of 0.116 Hz).

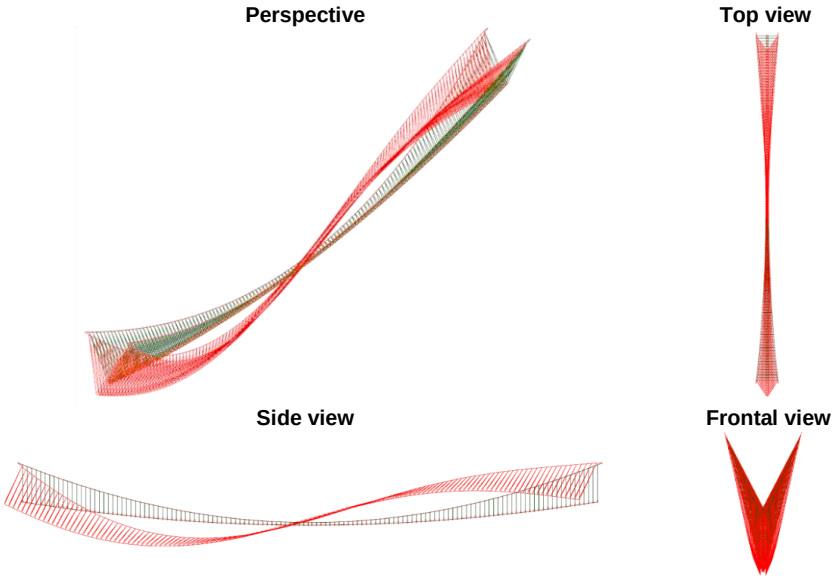

Figure 10: First in-plane mode shapes obtained numerically be the FE model (frequency of 0.157 Hz).

Tables 2 and 3 summarise the natural frequencies, the modal damping ratios, and the natural frequencies provided by the FE model for in-plane and out-of-plane mode shapes. The estimated standard deviations of both natural frequencies and damping ratios are also included. Furthermore, the complexity of the mode shapes is low, which shows measurements and modal

parameter estimation are correct and the structure presents proportional damping. The identification frequency range is limited by the number of sensors in the bridge.

The FE model reliably predicts the natural frequencies of the first-mode shapes. The Modal Assurance Criterion (MAC) [38] between the experimental and numerical mode shapes is also presented in Tables 3 and 4. A good agreement was obtained between the natural frequencies obtained from the finite element model and the experimental results, with maximum errors respectively below 22% and 10% for in-plane and out-of-plane mode shapes. The identified mode shapes have a cumulative mass fraction of approximately 82% and 95% for in-plane and out-of-plane mode shapes. The MAC diagonal value is greater than 0.8 in all cases, except for the sixth in-plane, and the third out-of-plane modes, probably because they were not properly excited by the wind action and also due to the uncertainties in the cable tension. As for the sixth symmetric in-plane mode, the difference is more significant because the FE model cannot accurately handle the additional tension induced in the cable when this mode is excited.

In addition, two torsional modes at 0.407 Hz and 0.476 Hz were identified with damping ratios equal to 0.914% and 0.945%, respectively. These mode shapes could contribute to the structural response in the case of vandalism, such as when a group of people provoke the movement from the upstream to the downstream side, thus inducing a swinging motion.

The mode shapes are represented in Figures 11 and 12. However, the identified mode shapes are limited by the number of measurement points.

Table 3: Summary of in-plane (vertical) mode shapes and the estimated natural frequencies f_{Exp}, modal damping ratios ζ, complexity, and modal masses m_{Exp}. The natural frequencies f_{FE} of the FE model and the MAC value are also shown.

F_{Exp} [Hz]	Standard deviation [Hz]	Complexity [%]	f_{FE} [Hz]	MAC [-]	ξ [%]	Standard deviation [%]	m_{Exp} [kg]
0.147	0.53E-6	0.059	0.157	0.999	1.05	0.032	18228
0.214	1.39E-6	0.012	0.249	0.994	0.70	0.017	9815
0.302	0.58E-6	0.047	0.350	0.986	0.55	0.008	11217

0.364	2.13E-6	0.027	0.418	0.949	0.64	0.004	12132
0.443	2.59E-6	0.164	0.526	0.975	0.52	0.004	11513
0.504	1.18E-6	0.303	0.617	0.581	0.57	0.005	16743
0.591	0.72E-6	19.863	0.691	0.917	0.35	0.007	10166
0.672	0.83E-6	0.126	0.789	0.959	0.41	0.006	6485
0.737	0.33E-6	0.943	0.874	0.986	0.16	0.001	6804
0.810	8.30E-6	0.818	0.961	0.956	0.78	0.023	4792
0.959	1.25E-6	0.395	1.130	0.983	1.15	0.006	4882
1.031	1.60E-6	3.27	1.217	0.973	0.87	0.008	6521
1.103	2.74E-6	2.536	1.300	0.917	0.58	0.003	5939

Table 4: Summary of out-of-plane (lateral) mode shapes and estimated natural frequencies f_{Exp} , modal damping ratios ζ, complexity, and modal masses m_{Exp}. The natural frequencies f_{FE} of the FE model and the MAC value are also shown.

F_{Exp} [Hz]	Standard deviation [Hz]	Complexity [%]	f_{FE} [Hz]	MAC [-]	ξ [%]	Standard deviation [%]	m_{Exp} [kg]
0.113	0.83E-6	0.006	0.116	0.951	1.45	0.035	60723
0.131	1.85E-6	42.127	0.135	0.853	1.65	0.080	51331
0.196	2.57E-6	0.145	0.205	0.585	1.48	0.050	20076
0.214	2.36E-6	0.832	0.221	0.979	0.84	0.029	38154
0.257	4.70E-6	1.326	0.267	0.966	1.65	0.037	44071
0.293	1.30E-6	0.569	0.311	0.973	0.91	0.022	37921
0.344	8.93E-6	0.214	0.356	0.945	0.95	0.010	26473
0.389	2.30E-6	0.45	0.402	0.953	0.90	0.006	31027
0.428	10.72E-6	0.085	0.451	0.967	0.63	0.007	31695
0.514	7.35E-6	17.173	0.544	0.869	0.87	0.025	16830
0.571	3.45E-6	4.602	0.633	0.969	0.63	0.011	26604

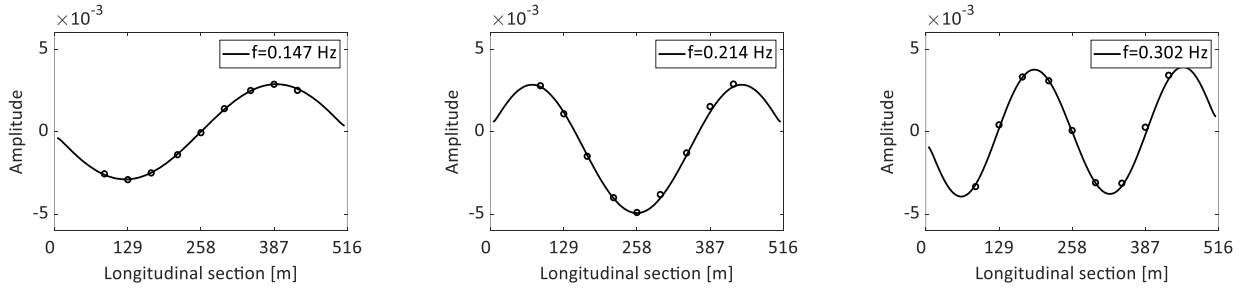

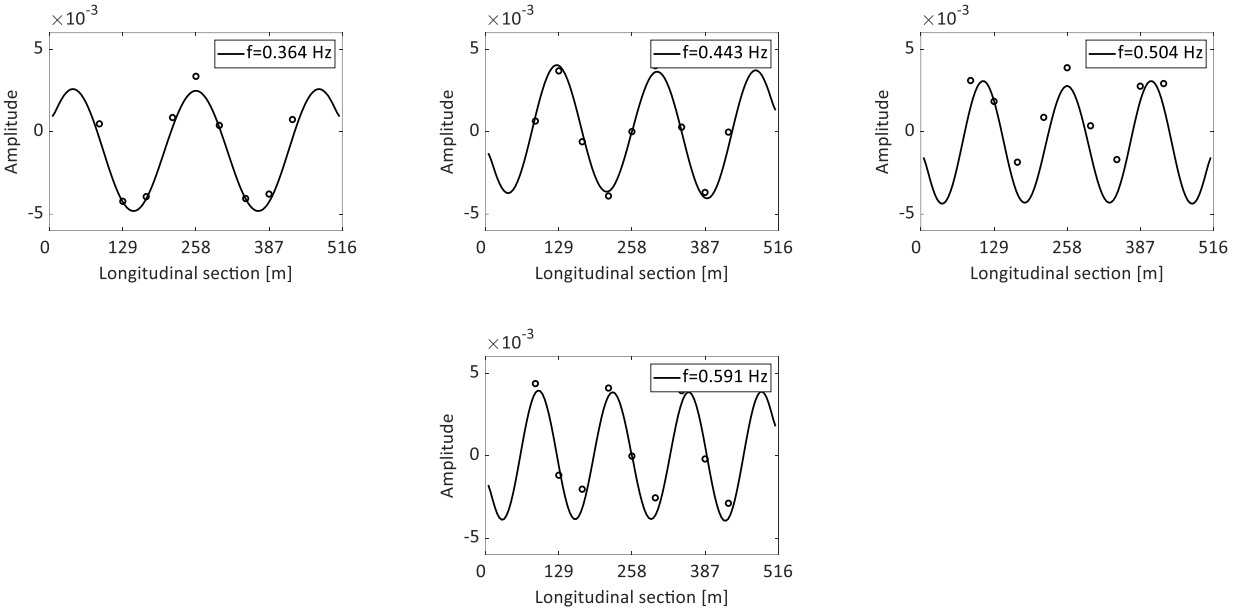

1 Figure 11: Experimental (circles) and numerical (solid line) in-plane mode shapes.

2

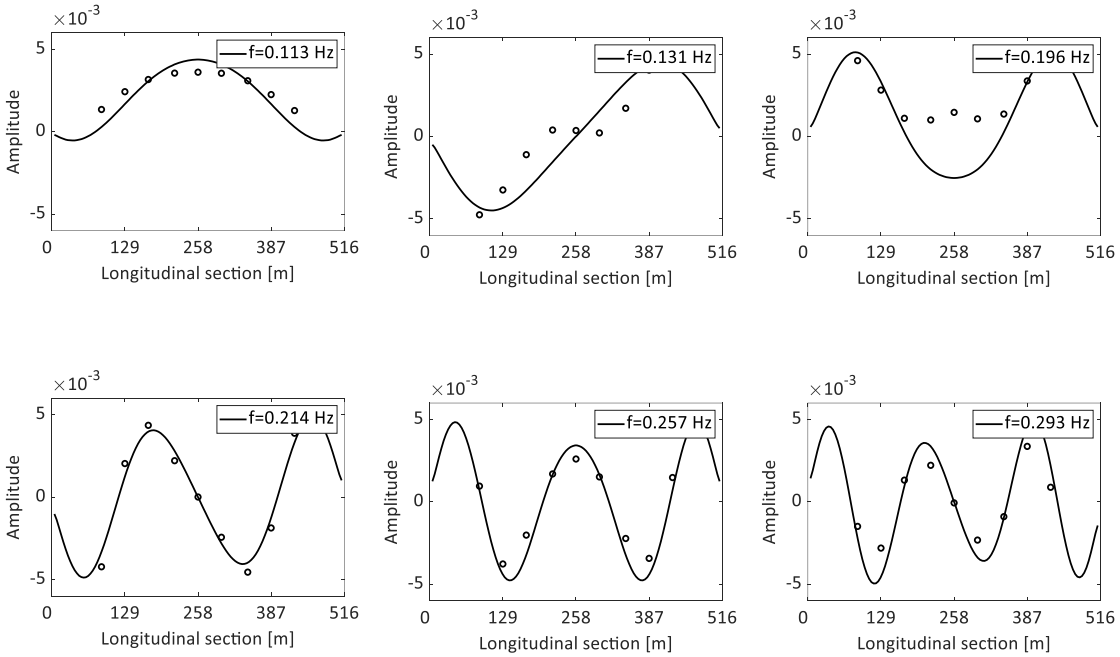

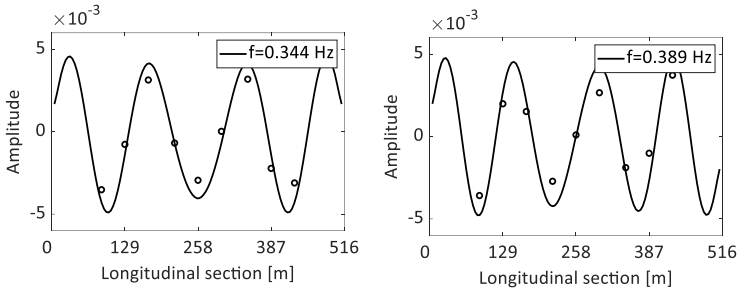

Figure 12: Experimental (circles) and numerical (solid line) out-of-plane mode shapes.

Additional computations have been performed to study the effect of the temperature variation on the natural frequencies. An increase in temperature of 30 ˚C was considered, which resulted in a length of the main cables of 532.214 m (additional 0.19 m) and a sag of 53.91 m. The FE model simulations lead to a small decrease of about 0.3% in the natural frequencies.

6.2 Dynamic response due to pedestrian loads

The power spectral density (PSD) of the acceleration at all instrumented sections was analysed to identify the natural frequencies excited by the pedestrian load. Obviously, the wind action was also active during this test. The PSD is obtained from the average of 8 segments of the original time series with 50% overlap applying a Hamming window [39]. The time responses at an upstream position of 1/3 of the bridge span (Position 3) during Test 1 is shown in Section 7. The analysis of the PSD allows identification of the mode shape that contributes to the structural response to pedestrian load.

Figures 13 and 14 show the PSD of the vertical and lateral accelerations recorded during the walking tests at section corresponding to L/3 (position 3). The PSD due to the wind action, recorded during a half-hour period, is also represented as a reference for the unloaded case. These figures also represent the maximum acceleration obtained numerically, provided by uniformly distributed loads computed for the 34 pedestrians and three different structural damping ratios (ξ=0.2%, ξ=2.0% and ξ=4.0%) according to the HiVoSS and SETRA guidelines.

These damping ratio values represent the range estimated from the measurements for the different tests and agree with those indicated by HiVoSS and SETRA (ξ=0.2% is, in any case, the minimum value, ξ=2.0% corresponded to welded steel structures, and ξ=4.0% is associated with bolted steel structures). The highlighted/shaded areas represent the critical ranges for natural frequencies of footbridges with pedestrian excitation for vertical and lateral vibrations, according to the HiVoSS and SETRA guidelines. Since the lateral vibrations are not affected by the second harmonic of pedestrian loads, only the vertical case (Figure 13) shows two ranges, (in the case of HiVoSS) corresponding to the first and second harmonics (see Figure 5).

The frequency contents show peaks at the natural frequencies identified in the SVD (Figure 8). The effect of the 34 pedestrians was found to reduce the lowest natural frequencies of the structure by around 2%. The acceleration levels produced by the pedestrian load are higher than those caused by the wind load, and a noticeable amplification is found in the critical ranges of natural frequencies represented between vertical dashed lines.

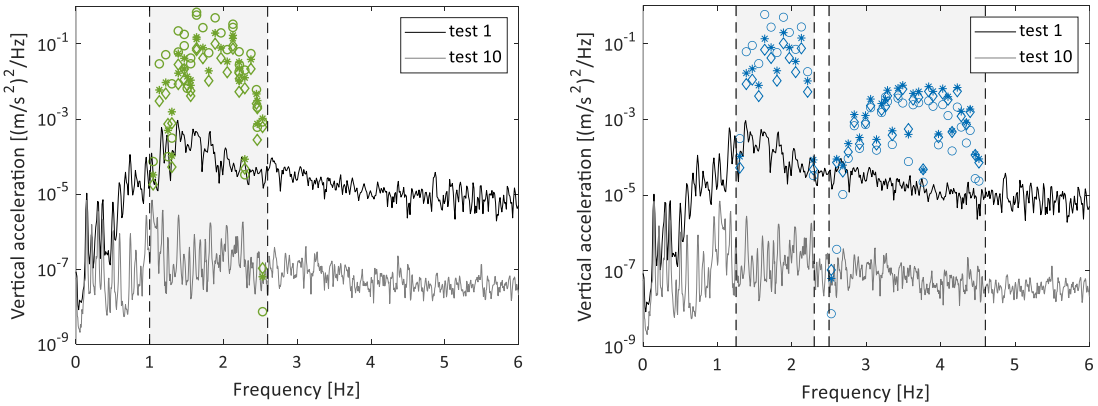

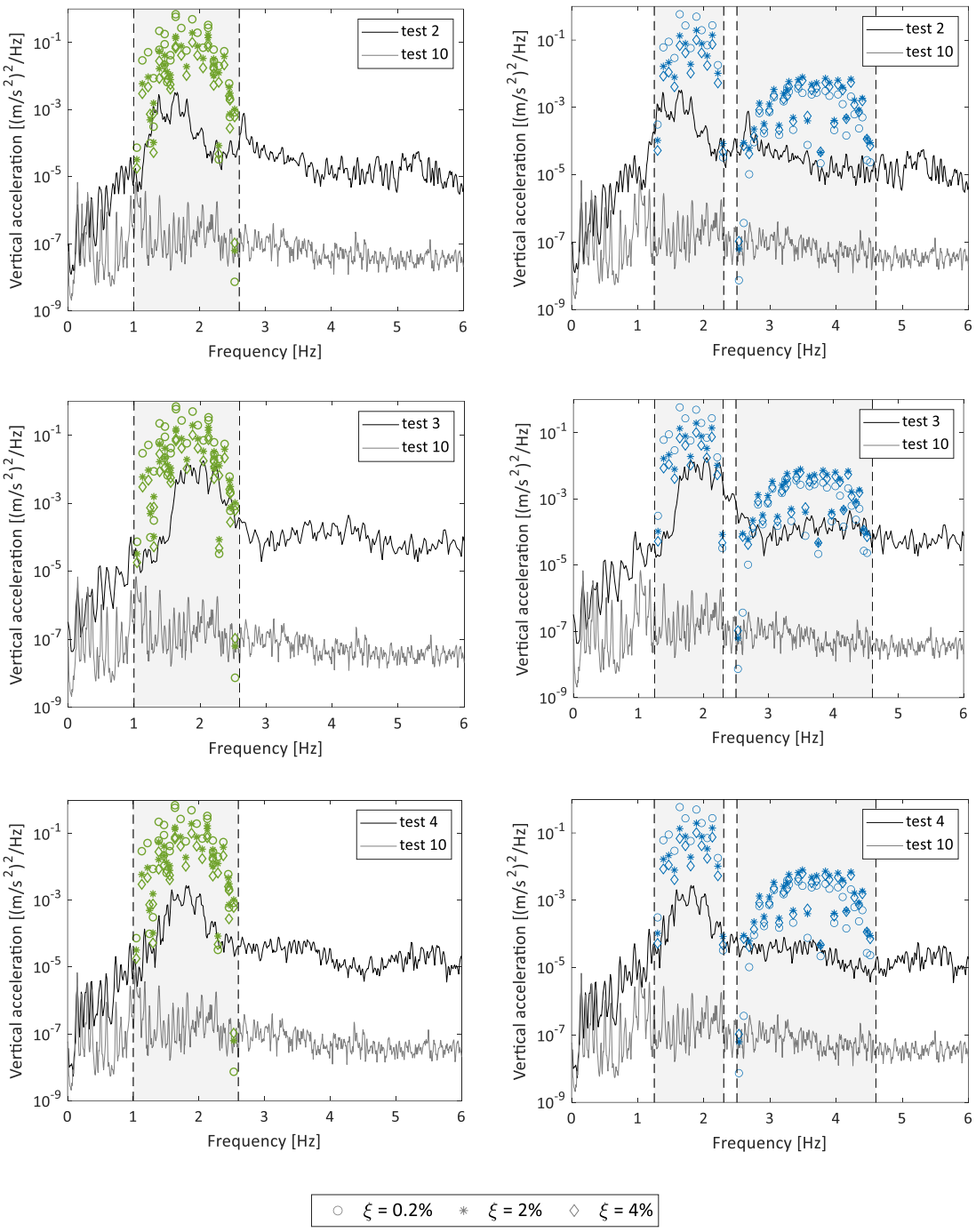

1 Figure 13: PSD of the vertical acceleration at the at section corresponding to L/3 (position 3) for the walking tests.

2 The critical ranges of natural frequencies are represented between vertical dashed lines: SETRA guideline (left);

3 HiVoSS guideline (right).

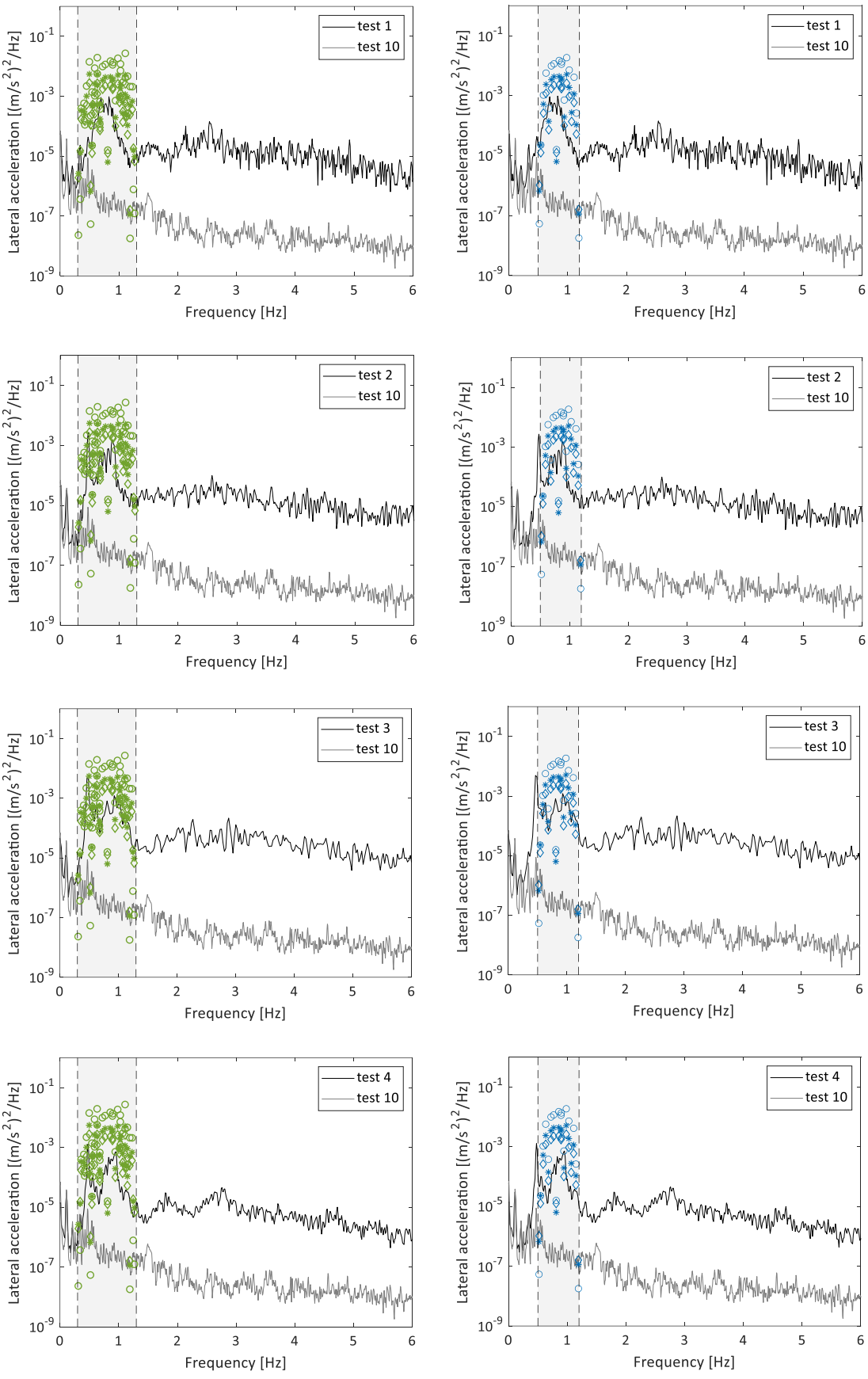
test 1
test 10
test 2
test 10
test 3
test 10
test 4
test 10
Lateral acceleration [(m/s^2)^2/Hz]
Frequency [Hz]
ξ = 0.2%
ξ = 2%
ξ = 4%

Figure 14: PSD of lateral acceleration at the at section corresponding to L/3 (position 3) for walking tests. The critical ranges of natural frequencies are represented between vertical dashed lines: SETRA guideline (left); HiVoSS guideline (right).

The frequency content of the vertical acceleration exhibits higher peaks at section corresponding to L/3 than at other measuring positions (not illustrated). In addition, a peak outside the critical range of natural frequencies is found at 2.67 Hz in Test 2, corresponding to the second harmonic of the pedestrian load obtained for a fixed pace of 1 m/s and from a representative step length of 0.7 m. Similarly, peaks at 1.69 Hz and their related second harmonic were found for a walking speed of 1.5 m/s (Test 3), which indicates that the pedestrian reduced the step length to 0.59 m to keep the pace. The response of the bridge due to a random pace (Test 4) is similar to the previous cases, but without a significant peak related to the load frequency.

The lateral component of the acceleration shows predominant peaks at 0.428 and 0.918 Hz, respectively, corresponding to the natural frequencies of the out-of-plane mode shapes.

The numerical acceleration levels computed according to the HiVoSS and SETRA guidelines are generally much higher than the measurements, which demonstrates the importance of performing experimental in situ tests to validate the structure's dynamic behaviour and to evaluate the human-structure interaction.

The load case scenarios required to be taken into consideration in the design phase are the main difference between the two guidelines. HiVoSS does not consider the second harmonic of the lateral load. SETRA does not consider the second harmonic for both directions (vertical and lateral), for the particular case of the pedestrian's density of this bridge (lower than 0.8). The results show that the second harmonic has little significance for the 516 Arouca bridge which only allows the presence of a limited number of pedestrians, in line with SETRA's assumptions. HiVoSS also states that at the date of its publication, the literature does not report the existence of onerous vertical vibrations in footbridges due to the second harmonic of pedestrians. The

numerical analysis also allows comparing the response of the bridge under different pedestrian loads.

As the second harmonic is only taken into account under the HiVoSS guideline, (for this pedestrian's density) the following analyses were only computed for this guideline. Figures 15 and 16 show the lateral and vertical acceleration, respectively, when the number of people on the bridge increases, assuming a damping ratio of 2%. The results show that increasing the number of people on the bridge increases acceleration.

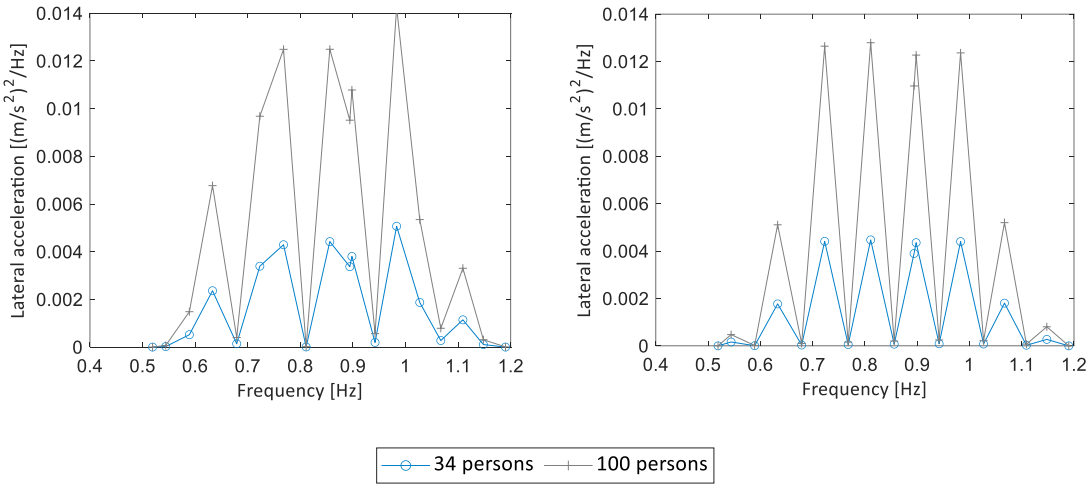

Figure 15: Lateral accelerations are computed numerically at positions 3 (left) and 5 (right) when 34 and 100 people are uniformly distributed along the bridge span, for a damping ratio of 2%.

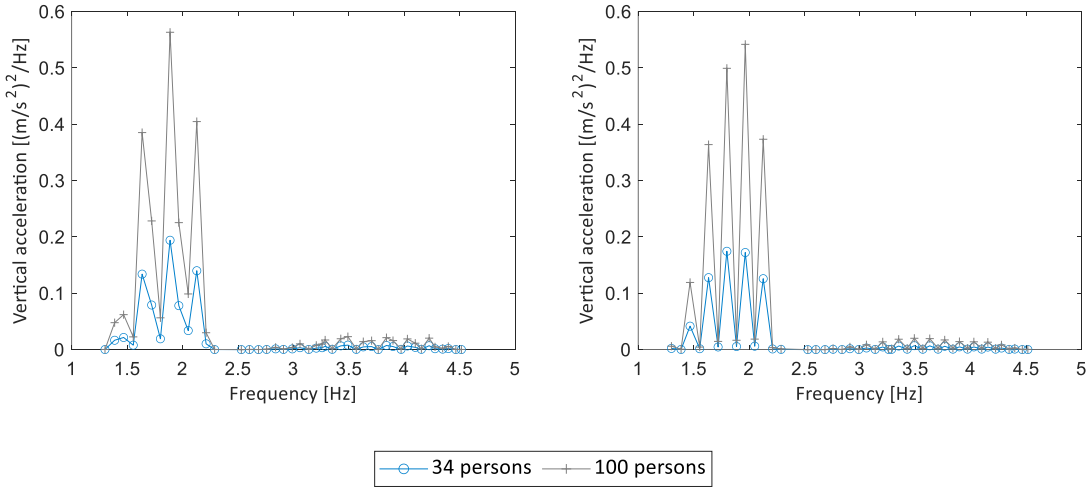

Figure 16: Vertical accelerations are computed numerically at positions 3 (left) and 5 (right) when 34 and 100 people are evenly distributed along the bridge span, for a damping ratio of 2%.

Another numerical analysis was performed comparing 34 people distributed uniformly throughout the bridge span and a load only distributed in the vicinity of the midspan module. The results show that the acceleration is almost the same, except for the vertical results at position 5 (midspan), where the acceleration increases slightly (see Figures 15 and 16).

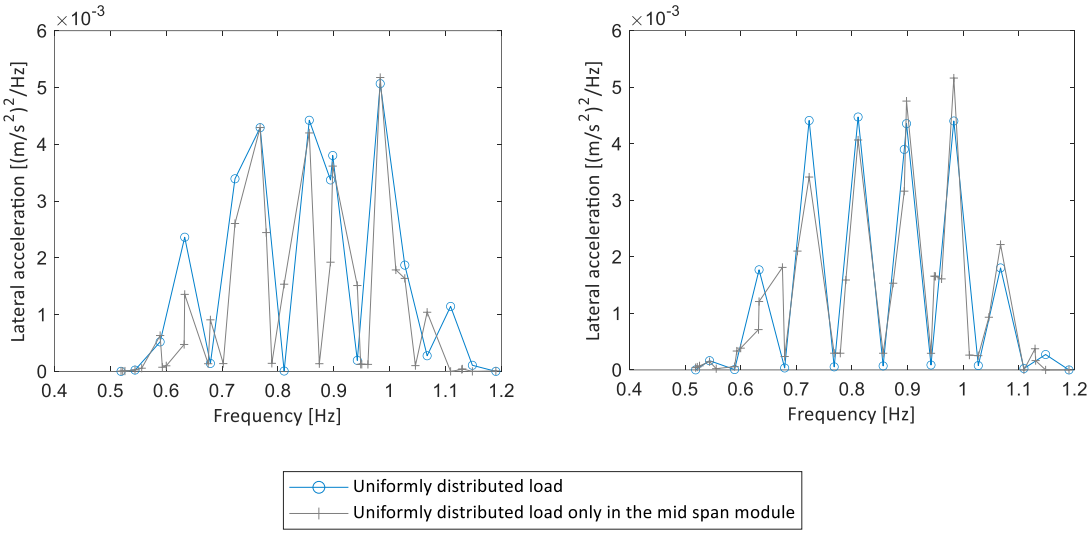

Figure 17: Lateral accelerations are computed at positions 3 (left) and 5 (right) for a load distributed uniformly along the bridge span and a load only distributed in the vicinity of the midspan module, for a damping ratio of 2%.

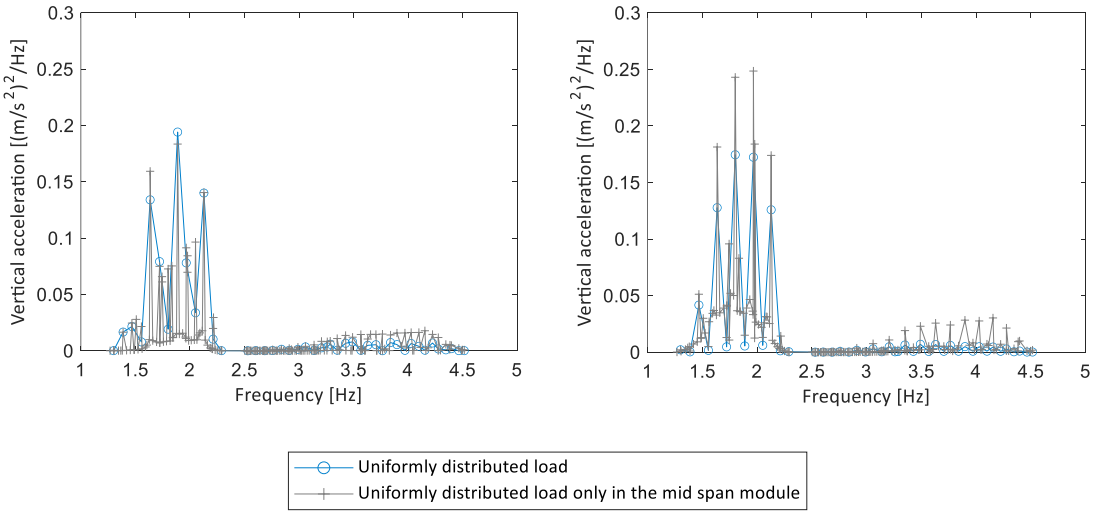

Figure 18: Vertical accelerations are computed at positions 3 (left) and 5 (right) for a load distributed uniformly along the bridge span and a load distributed only in the vicinity of the midspan module, for a damping ratio of 2%.

6.3 Structural response due to vandal loading

The dynamic analysis of the structural response to vandal loading is presented in this section. This analysis covers the pedestrian running, jumping, and swinging tests. These tests aimed to excite the natural modes in all directions, but particularly the lateral and vertical directions.

The running test at a fixed pace of 2.5 m/s mainly excites the seventh in-plane and sixth out-of-plane mode shapes with natural frequencies of 0.672 and 0.389 Hz, respectively (see Figure 19). The frequency content of the lateral acceleration also shows peaks at 0.964 Hz related to a high-order out-of-plane mode shape, and its related high-order harmonics to the mode shape at 0.389 Hz. This effect is not observed for the vertical acceleration.

The vertical and lateral acceleration levels recorded during Test 5 were lower than those due to pedestrian loads (Tests 1-4). The numerical predictions match those presented in the previous section since the dynamic load of the HiVoSS and SETRA guidelines does not depend on the pace.

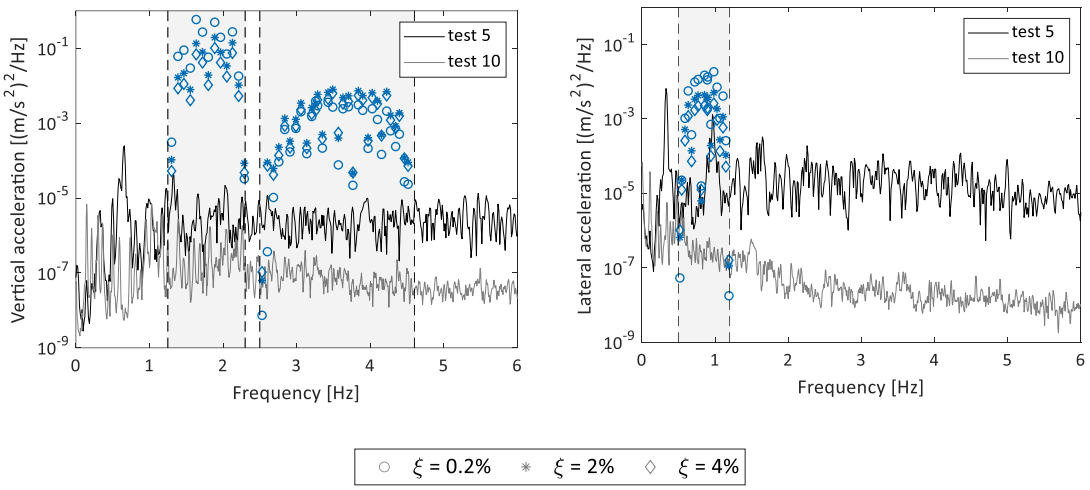

Figure 19: PSD of the vertical (left) and lateral (right) acceleration components at the at section corresponding to L/3 (position 3) for the running test. The wind response (Test 10) is represented as a reference. The comfort limit ranges of natural frequencies defined by the HiVoSS guidelines are represented between vertical dashed lines.

The damping ratios of these mode shapes are compared with the crossing tests at a slower walking speed. Table 5 shows the modal damping ratios for the in-plane mode shape at 0.672 Hz and the out-of-plane one at 0.389 Hz. Since the bridge response induced by the walking loads

was attenuated in a short time for some of the tests (see Table 5) and the estimations using EFDD require longer records, the half-power bandwidth method [40] was used to identify the modal damping in all cases for comparison purposes. The damping ratios estimated from the wind action response by EFDD are in brackets (see Tables 3 and 4). The damping ratios increase with the pace of walking as the structural response increases, highlighting the dependence of the damping ratio on the amplitude of the structural response.

Table 5: Modal damping ratio [%] for different tests estimated from the half-power bandwidth method. The damping ratios estimated from the wind response by the EFDD are in brackets. The time span is also indicated for each test.

Mode shape	Test 1 (1135 s)	Test 2 (807 s)	Test 3 (600 s)	Test 5 (283 s)	Test 10 (1800 s)
0.389 Hz	0.9	1.4	2.7	3.3	0.7 (0.90)
0.672 Hz	0.5	0.7	1.4	1.6	0.4 (0.41)

Figure 20 shows the bridge response at the midspan for the jumping tests. The load produced by the jumps excites a large number of in-plane mode shapes, causing a large amplification of the response compared to the wind load. The frequency content of the response presents a distribution similar to a step load function, where the distance between two consecutive minima corresponds to the inverse of the time-step load. In this case, the maxima are reached around 1.25 Hz, and local maxima are observed at 2.7 Hz for Test 6 (jumping at L/4), and 3.2 Hz for Test 7 (jumping at L/3). The time-step load can be estimated as 0.66 s and 0.74 s for each test, respectively.

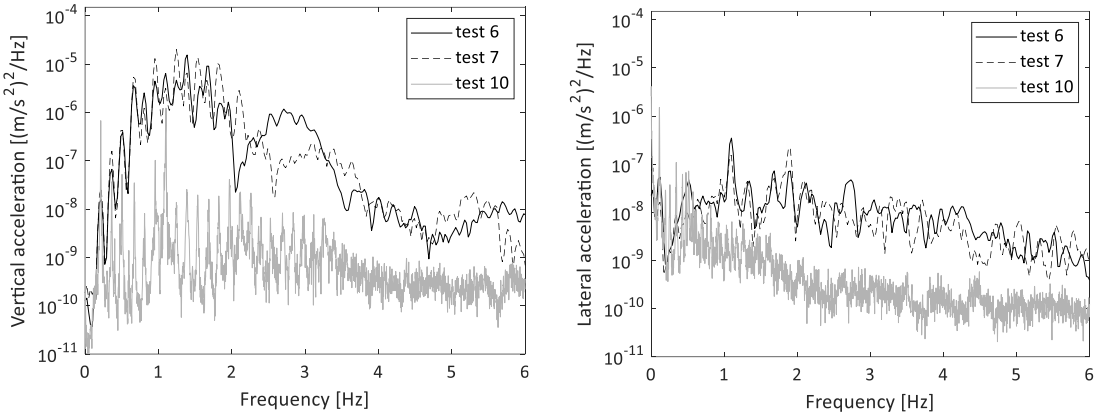

Figure 20: PSD of (a) the vertical and (b) the lateral acceleration components at midspan for jumping tests. The wind response (Test 10) is represented as a reference.

Finally, Figure 21 shows the acceleration at the midspan upstream and downstream positions (positions 5 and 10, respectively) for the swing tests. The frequency content shows a similar pattern to those of the jumping tests. The maximum response occurs in the vertical component and is similar at the upstream and downstream positions, although the response at position 5 is higher than at position 10 for high frequencies. The identified torsional mode shape at 0.407 Hz was not detected, and it can be concluded that it was not excited during the tests.

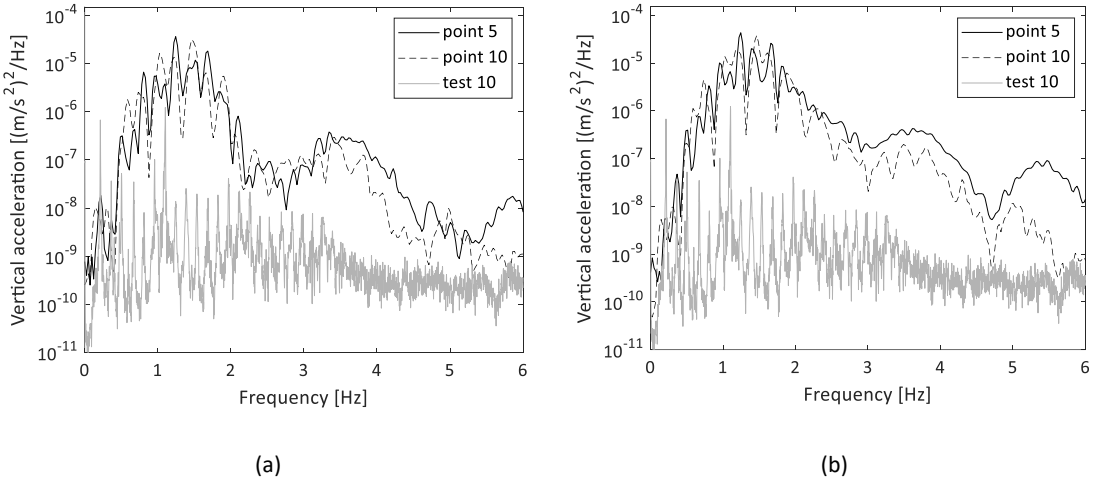

Figure 21: PSD of the vertical acceleration component at midspan for swinging tests (a) 8 and (b) 9. The wind response (Test 10) is represented as a reference.

7- Assessment of comfort classes

The assessment of pedestrian comfort is commonly represented as the limit acceleration for the footbridge, and the perception of motion and vibration are subjective and therefore different for each pedestrian [13]. The analyses of the comfort class for the walking tests are discussed. Special attention was paid to the human perception of the vibration of the footbridge. A questionnaire was prepared, designed to be answered by the first groups of people who visited the bridge after the opening so as to learn their thoughts on the experience of crossing the footbridge. A total of 1030 visitors completed the questionnaire.

The assessment of the comfort classes allows us to define the time percentage of the response that exceeds the acceleration limits [13]. The vibration was continuously measured by all seismometers. The maximum response at the measurement positions was recorded when the group of pedestrians was near a seismometer. The vibration level gradually decreases over time. Therefore, to evaluate the comfort classes, a representative interval of the response is defined as the time period around the maximum level of acceleration that exceeds a noise level. This level is obtained as the mean value of the acceleration in a time window of 4 seconds around the maximum response.

Given the amount of recorded data, Test 1 is used to illustrate the performed analysis. All other results are summarised in figures, most of which can be found in the supplementary material.

Figure 22 (a-c) shows the acceleration responses at an upstream position of the bridge midspan (Position 3) when the group of 34 people crossed the bridge from one side to the other side at a slow pace of 0.5 m/s (1.8 km/h). Each plot includes the acceleration limits following the European guideline HiVoSS [13].

As expected, larger acceleration amplitudes are observed at each seismometer when the group of volunteers was moving in its vicinity. In addition, the displacements recorded by the

GNSS antennas on the X (longitudinal direction), Y (vertical direction), and Z (lateral direction)-axes are presented (Figure 23). As expected, the transversal displacement is very low given that the wind speed was below 3.0 m/s, and the people moved slowly. As can be seen, the middle platform module had a maximum Y-axis displacement of 0.48 m, a maximum X-axis displacement of 0.12 m, and a Z-axis displacement of 0.06 m.

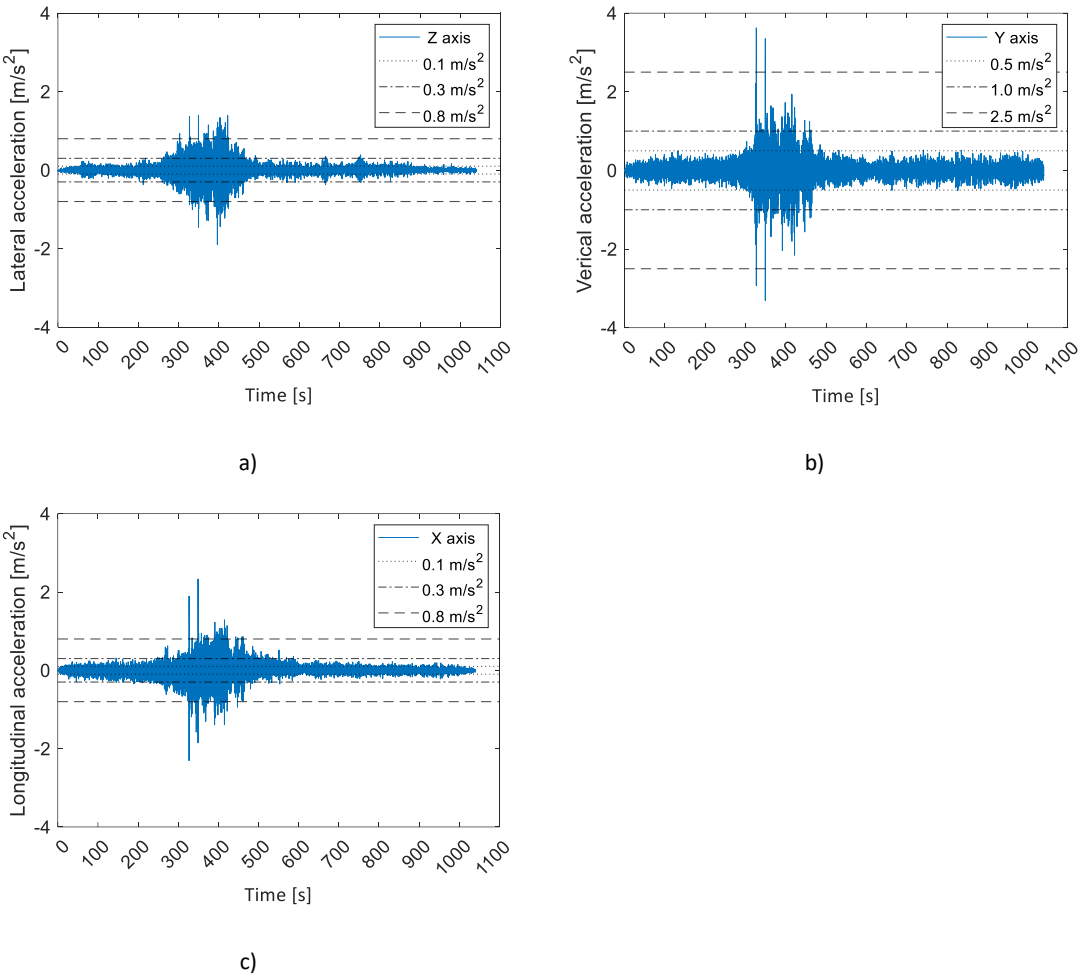

1 Figure 22: Test 1 – Walking on the bridge at 0.5 m/s (1.8 km/h) - position 3 upstream of the bridge span for: a)

2 Longitudinal acceleration (X-axis); b) Vertical acceleration (Y-axis); c) Lateral acceleration (Z-axis).

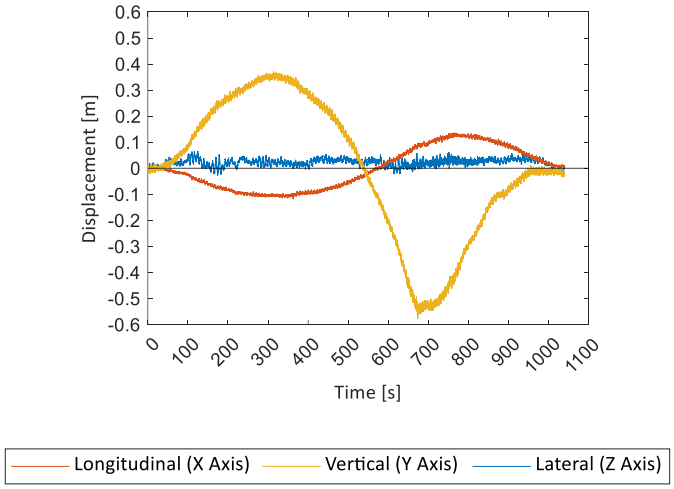

3 Figure 23: Test 1 – Walking on the bridge at 0.5 m/s (1.8 km/h) - at the at section corresponding to 2L/3 (position 7)

4 for X-, Y- and Z-axis displacement recorded by the GNSS antenna.

The analysis of these results allowed us to evaluate the total time for which each comfort level was sensed for the three axes (see Figure 24:). These acceleration ranges and percentages for all monitoring positions and for all walking tests (Tests 2 to 4), are presented in the supplementary material. The comfort level can be classified as maximum or medium most of the time, according to the ranges represented, especially in the vertical direction. The percentage of time for which the acceleration was at uncomfortable levels was almost zero for Test 1.

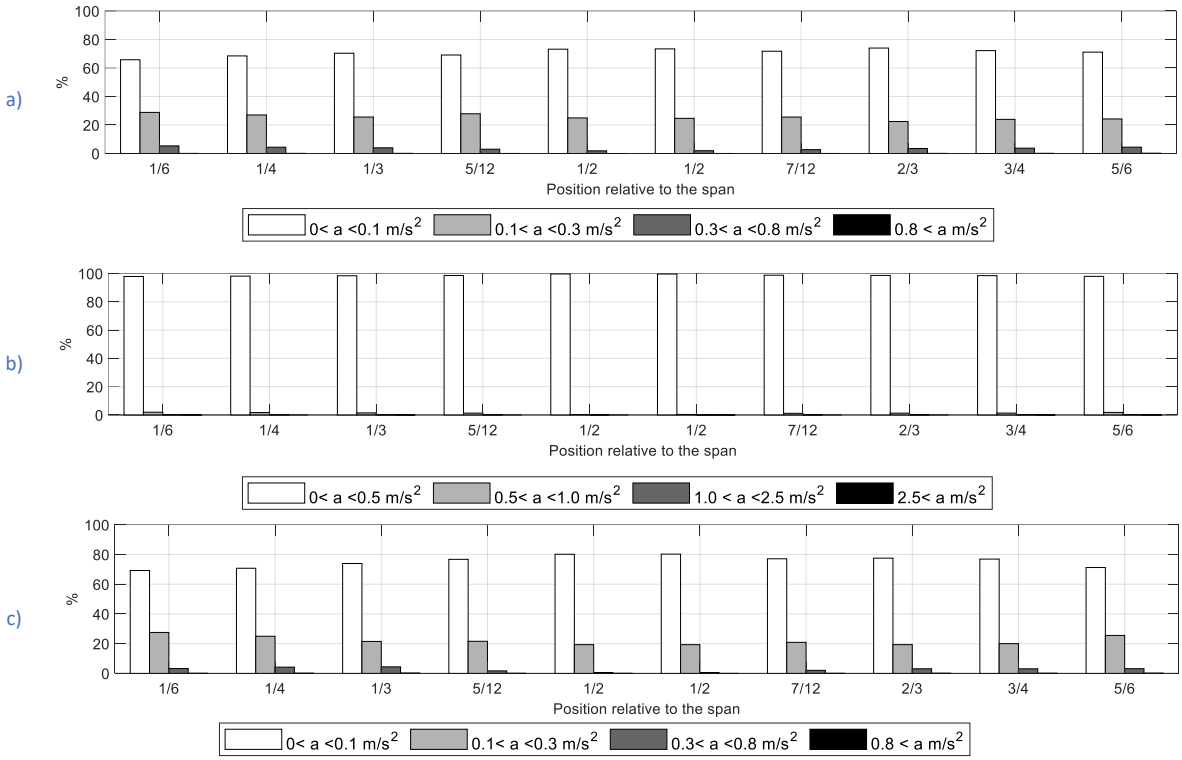

Figure 24: Acceleration ranges and percentages, for all monitoring positions, obtained during Test 1: a) X axis (longitudinal direction); b) Y axis (vertical direction); c) Z axis (lateral direction).

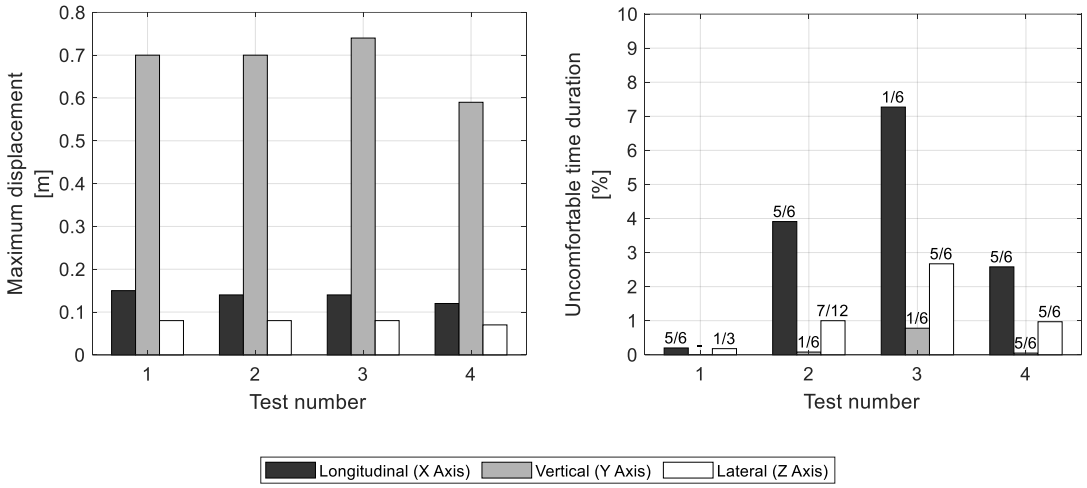

a) b)

Figure 25: Analysis of the tests: a) Maximum displacement recorded by the GNSS antennas; b) Total time percentage and the position at which the uncomfortable level limit was highest.

The maximum displacements, recorded by the GNSS antennas, (Figure 25: a) for the walking tests (Tests 1- 4) are 0.74 m, 0.13 m, and 0.08 m for the vertical, transverse, and longitudinal directions, respectively. These correspond to 1/697, 1/3969, and 1/6450 of the bridge span, which are considered very small fractions. For the jumping tests, the maximum displacement was below the values recorded for the walking tests, with the vertical and longitudinal directions registering 0.35 m and 0.12 m, respectively. In the lateral direction, the maximum value was 0.03 m.

As can be seen, the results corroborate the previous analysis done for Test 1; the faster the pace, the greater the acceleration provoked by the pedestrian excitation. Analysis of these results also leads to the conclusion, as expected, that higher frequency spectra amplitudes are associated with the frequencies excited by the movement of the group. Test 4 (random pace) corresponds to the behaviour expected of the public on the bridge. The results show that the acceleration values are very low and the discomfort level can be assumed to be nearly negligible (Figure 25: b).

7 Human perception

Human perception of footbridge vibration in general is a combination of movement of the system, physical perception, and psychological reaction to vibration. Occupants in various settings will be more sensitive to exactly the same vibration than others, depending on the frequency of occurrence, duration, and time of day. According to Grether [41], humans are more sensitive to vertical vibrations in the frequency range of 4–8 Hz due to resonance phenomena within the body itself. In addition, human perception depends on the activity of a person at the time of the perceived event.

The classification of uncomfortable vibrations is very subjective. Determining acceptability can be a challenge due to the large number of factors upon which vibration perception depends. The bridge visitors anonymously responded to a questionnaire. Between the opening and the submission of this paper, 1030 people responded to the inquiry about the experience, Figure 26. The questionnaire was available in Portuguese, Spanish, English, and French and was provided by the bridge guide, who invited people to answer it at the end of the bridge tour. The survey questions are presented in the supplementary material.

The survey given to visitors starts by asking if the person feels fear during the crossing. 84.8% answered no. The visitors are then asked about the comfort level perceived during the crossing, with four options given for comfort class maximum, medium, minimum, and unacceptable, associated respectively with practically imperceptible vibration, merely perceptible vibration but not unpleasant, perceived vibration but not intolerable and intolerable. The results show that 59% of the surveyed visitors chose the maximum comfort option, 38% chose medium comfort, and 2.1% and 0.9% classified vibration comfort as minimum and unacceptable, respectively, which is in accordance with the vibration assessment presented in the previous section. People were also asked if they felt safe; 96.1% said yes.

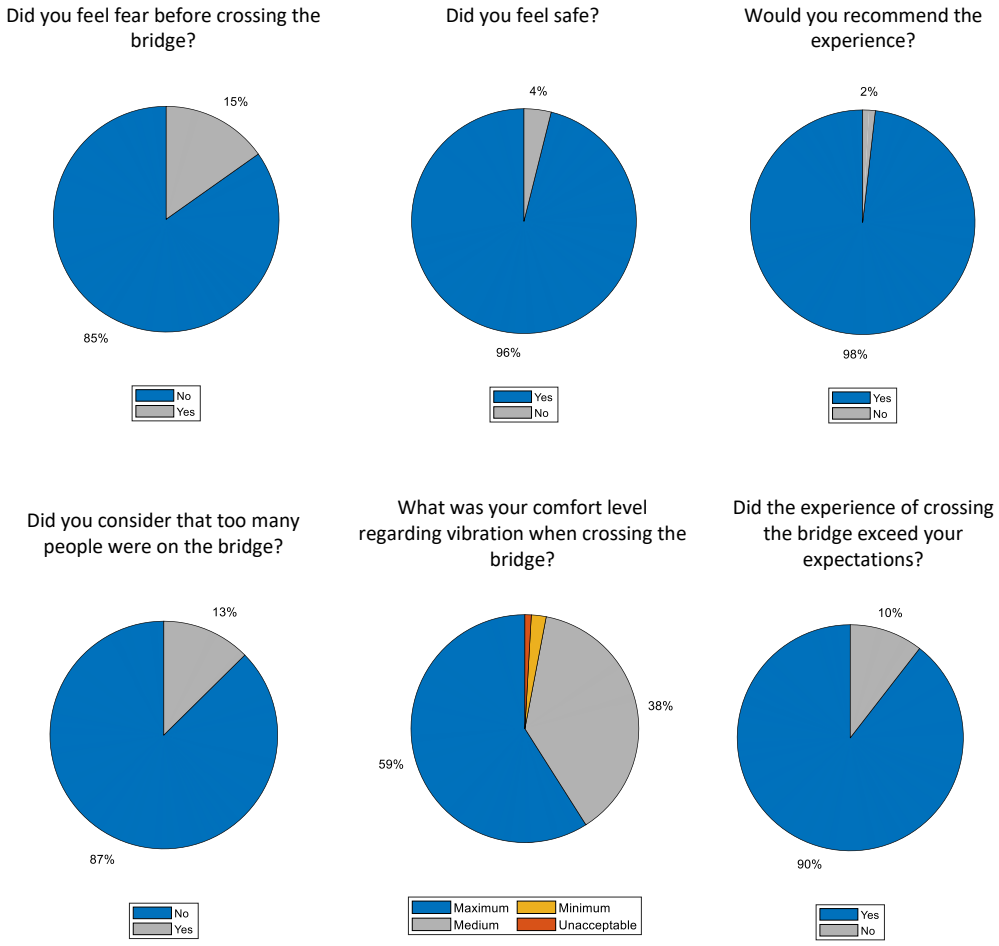

Figure 26: Volunteers' answers.

8- Conclusions

This paper has investigated the vibrations and displacements induced by the wind and humans through in situ behaviour tests on the 516 Arouca pedestrian bridge in Portugal. The tests were carried out by a group of 34 people, which is 2778 kg of total mass on the footbridge. Bridge responses caused by people crossing (walking at different speeds), running, jumping, and swinging (simulating a deliberately harmful action) were recorded. All tests were performed under similar very low wind conditions.

Some major conclusions can be drawn from the research work:

- The evaluated mode shapes and corresponding natural frequencies were found to be similar to those previously computed by a finite element model at the design stage.
- The damping ratios were found to be appropriate for the present lighter, slender bridge. These increase with the pace of walking, as the structural response increases, highlighting the dependence of the damping ratio on the amplitude of the structural response.
- European guidelines (HiVoSS and SETRA) were used to compute numerical acceleration levels. The results, obtained for three different damping ratios (0.2%, 2%, and 4%) were found to be much higher than the acceleration measurements.
- The effect of the 34 pedestrians was found to reduce the lowest natural frequencies of the structure by around 2%.
- The use of GNNS antennas seems to be a suitable way to measure the static behaviour of this type of bridge. The maximum displacements recorded by those for the walking tests were 0.74 m, 0.13 m, and 0.08 m for the vertical, transverse, and longitudinal directions, respectively. These correspond to 1/697, 1/3969, and 1/6450 of the bridge span, which are considered very small fractions.
- The effect of the temperature variation on the natural frequencies of the bridge is minimal and thus can be neglected.
- The acceleration levels produced by the pedestrians had a noticeable amplification, found in the critical ranges of natural frequencies indicated in the guidelines (HiVoSS and SETRA). Peaks outside the critical range of natural frequencies were also found and correspond to the second harmonic of the pedestrian load.
- The lateral component of the acceleration shows predominant peaks corresponding to the natural frequencies of the out-of-plane mode shapes.

- The amount of time for which the acceleration limits, imposed by the HIVOS and SETRA guidelines, were exceeded was calculated. The results demonstrate that depending on the test type, the acceleration levels may vary. Higher accelerations happen when pedestrians jump simultaneously on the bridge or produce a swinging motion, which is not allowed and therefore considered uncommon.
- The damping ratios were found to increase with the pace of walking as the response of the structural response increased, highlighting the dependence of the damping ratio on the amplitude of the structural response. A damping of 2% was reached when a group of 34 people walked on the bridge.
- The survey results contribute to assessing human sensitivity to the vibrations of this kind of bridge. 97% of visitors considered that the vibration could be classified as practically imperceptible vibration or slightly perceptible, showing that the visitors felt completely safe while on the bridge. Overall, the results show that the comfort limits defined in the European guidelines (HiVoSS and SETRA) are suitable for this type of bridge.

Acknowledgments

The authors would like to acknowledge the support provided by Arouca City Hall (Câmara Municipal de Arouca), with special thanks to the mayor, Margarida Belém, and the Council Engineer Conceição Oliveira; to the group of 34 volunteers for their time and patience; to José Rego for the photos; to the Portuguese enterprises MEO - Serviços de Comunicações e Multimédia, SA, and Geoide Geosystems SA, for the internet connection and GNS antennas data, respectively; to LNEC (National Laboratory of Civil Engineering) for the anemometer data and their help in the group and work coordination. Finally, the authors would also like to

acknowledge the financial support provided by the Spanish Ministry of Science, Innovation and Universities (PID2019-109622RB-C21).

References

[1] S. R, "The influence of human occupants on the dynamic properties of slender structures," University of Sheffield, 2002.

[2] P. Kumar and A. Kumar, "Human induced vibrations in structures," *Int. J. Mech. Eng. Robot. Res.*, vol. 1, no. 1, pp. 44–54, 2014.

[3] R. Sachse, A. Pavic, and P. Reynolds, *Human-structure dynamic interaction in civil engineering dynamics: A literature review*, vol. 35, no. 1. 2003.

[4] M. Huang, "Dynamic Characteristics of Slender Suspension Footbridges," no. May, p. 268, 2006.

[5] E. T. Ingólfsson, C. T. Georgakis, and J. Jönsson, "Pedestrian-induced lateral vibrations of footbridges: A literature review," *Eng. Struct.*, vol. 45, pp. 21–52, 2012, doi: 10.1016/j.engstruct.2012.05.038.

[6] S. Ali, D. Thambiratnam, X. Liu, and S. Fawzia, "Numerical study of pedestrian suspension bridge with innovative composite deck," *Heliyon*, vol. 6, no. 7, p. e04473, Jul. 2020, doi: 10.1016/j.heliyon.2020.e04473.

[7] "BS 5400 Steel, concrete and composite bridges - Part 2: Specifications for loads," 1978.

[8] "EN 1995-2:1997 Eurocode 5: Design of timber structures. Bridges," 1997.

[9] "CAN/CSA-S6-00 Canadian Highway Bridge Design Code," 2000.

[10] "DIN-Fachbericht 102 Concrete bridges," 2003.

[11] M. Schlaich, K. Brownlie, J. Cozett, J. Sobrino, J. Stráský, and K. Takenouchi, *fib Bulletin No. 32 - Guidelines for the design of footbridges*, no. December. e International

Federation for Structural Concrete, 2005.

[12] SETRA, “Footbridges - Assessment of vibrational behaviour of footbridges under pedestrian loading,” 2006.

[13] HiVoSS, “Design of Footbridges : Guideline,” 2007.

[14] C. Heinemeyer *et al.*, “Design of Lightweight Footbridges for Human Induced Vibrations,” Luxembourg, 2009.

[15] J. F. Jiménez-Alonso and A. Sáez, “Recent Advances in the Serviceability Assessment of Footbridges Under Pedestrian-Induced Vibrations,” in *Bridge Engineering*, InTech, 2018.

[16] C. Z. Dong, S. Bas, and F. N. Catbas, “Investigation of vibration serviceability of a footbridge using computer vision-based methods,” *Eng. Struct.*, vol. 224, Dec. 2020, doi: 10.1016/j.engstruct.2020.111224.

[17] F. A. Rezende, W. D. Varela, E. M. L. Carvalho, and A. M. B. Pereira, “Vibration performance assessment of a long-span steel footbridge,” *Proc. Inst. Civ. Eng. Struct. Build.*, vol. 175, no. 6, pp. 500–512, Jun. 2022, doi: 10.1680/jstbu.19.00184.

[18] K. Van Nimmen, J. Van Hauwermeiren, and P. Van den Broeck, “Eeklo Footbridge: Benchmark Dataset on Pedestrian-Induced Vibrations,” *J. Bridg. Eng.*, vol. 26, no. 7, Jul. 2021, doi: 10.1061/(asce)be.1943-5592.0001707.

[19] F. Venuti and F. Tubino, “Human-induced loading and dynamic response of footbridges in the vertical direction due to restricted pedestrian traffic,” *Struct. Infrastruct. Eng.*, vol. 17, no. 10, pp. 1431–1445, 2021, doi: 10.1080/15732479.2021.1897630.

[20] A. Tadeu, F. Marques da Silva, B. Ramezani, A. Romero, L. Škerget, and F. Bandeira, “Experimental and numerical evaluation of the wind load on the 516 Arouca pedestrian suspension bridge,” *J. Wind Eng. Ind. Aerodyn.*, vol. 220, p. 104837, Jan. 2022, doi:

10.1016/j.jweia.2021.104837.

[21] A. Tadeu *et al.*, “Theoretical and experimental analysis of the quasi-static and dynamic behaviour of the world’s longest suspension footbridge in 2020,” *Eng. Struct.*, vol. 253, p. 113830, Feb. 2022, doi: 10.1016/j.engstruct.2021.113830.

[22] R. G. Cuevas, J. F. Jiménez-Alonso, F. Martínez, and I. M. Díaz, “Uncertainty-based approaches for the lateral vibration serviceability assessment of slender footbridges,” *Structures*, vol. 33, pp. 3475–3485, Oct. 2021, doi: 10.1016/j.istruc.2021.06.055.

[23] R. E. White, N. A. Alexander, J. H. G. Macdonald, and M. Bocian, “Characterisation of crowd lateral dynamic forcing from full-scale measurements on the Clifton Suspension Bridge,” *Structures*, vol. 24, pp. 415–425, Apr. 2020, doi: 10.1016/j.istruc.2019.11.012.

[24] Q. Zhu, W. Yang, Y. Du, and S. Živanović, “Investigation of a vibration mitigation method based on crowd flow control on a footbridge,” *Structures*, vol. 33, pp. 1495–1509, Oct. 2021, doi: 10.1016/j.istruc.2021.05.034.

[25] K. Van Nimmen, A. Pavic, and P. Van den Broeck, “A simplified method to account for vertical human-structure interaction,” *Structures*, vol. 32, pp. 2004–2019, Aug. 2021, doi: 10.1016/j.istruc.2021.03.090.

[26] Y. B. Yang, J. D. Yau, and S. Urushadze, “Scanning the modal coupling of slender suspension footbridges by a virtual moving vehicle,” *Eng. Struct.*, vol. 180, pp. 574–585, Feb. 2019, doi: 10.1016/j.engstruct.2018.08.096.

[27] P. Dey, S. Narasimhan, and S. Walbridge, “Evaluation of Design Guidelines for the Serviceability Assessment of Aluminum Pedestrian Bridges,” *J. Bridg. Eng.*, vol. 22, no. 1, Jan. 2017, doi: 10.1061/(ASCE)BE.1943-5592.0000983.

[28] M. Setareh, “Vibration Serviceability Issues of Slender Footbridges,” *J. Bridg. Eng.*, vol. 21, no. 11, Nov. 2016, doi: 10.1061/(asce)be.1943-5592.0000951.

[29] L. Cao and J. Chen, “Online investigation of vibration serviceability limitations using smartphones,” *Meas. J. Int. Meas. Confed.*, vol. 162, p. 107850, 2020, doi: 10.1016/j.measurement.2020.107850.

[30] Autodesk, “Autodesk Robot Structural Analysis Professional.” 2020.

[31] “SYSCOM MR3000C.” https://www.syscom.ch/documentations/datasheet-mr3000c-english (accessed Mar. 14, 2022).

[32] “Leica model GS15 .” https://w3.leica-geosystems.com/downloads123/zz/gpsgis/viva gs15/brochures-datasheet/leica_viva_gs15_ds_en.pdf (accessed Mar. 14, 2022).

[33] “Gill windsonic 2D.” http://gillinstruments.com/data/datasheets/windsonic-1405-027-iss7.pdf (accessed Mar. 14, 2022).

[34] R. Brincker, L. Zhang, and P. Andersen, “Modal identification of output-only systems using frequency domain decomposition,” *Smart Mater. Struct.*, vol. 10, no. 3, pp. 441–445, Jun. 2001, doi: 10.1088/0964-1726/10/3/303.

[35] M. L. Aenlle and R. Brincker, “Modal scaling in operational modal analysis using a finite element model,” *Int. J. Mech. Sci.*, vol. 76, pp. 86–101, Nov. 2013, doi: 10.1016/j.ijmecsci.2013.09.003.

[36] M. L. Aenlle and R. Brincker, “Modal Scaling in OMA Using the Mass matrix of a Finite Element Model,” 2014, pp. 263–270.

[37] F. Pelayo, M. Aenlle, and R. Brincker, “Mass normalization of a 3D tubular structure combining operational modal analysis and a numerical model,” Sep. 2014, Accessed: Mar. 14, 2022. [Online]. Available: http://past.isma-isaac.be/downloads/isma2014/papers/isma2014_0633.pdf.

[38] R. J. Allemang and D. L. Brown, “Correlation coefficient for modal vector analysis,” in

International Modal Analysis I, Nov. 1982, pp. 110–116.

[39] S. Petre and M. Randolph, *Spectral Analysis of Signals Upper Saddle River*. Prentice Hall, 2005.

[40] D. J. Ewins, *Modal Testing: Theory, Practice and Application*, 2nd ed. 2009.

[41] W. F. Grether, “Vibration and Human Performance,” *Hum. Factors J. Hum. Factors Ergon. Soc.*, vol. 13, no. 3, pp. 203–216, 1971, doi: 10.1177/001872087101300301.

Supplementary Material

Acceleration ranges and percentages for the other walking tests

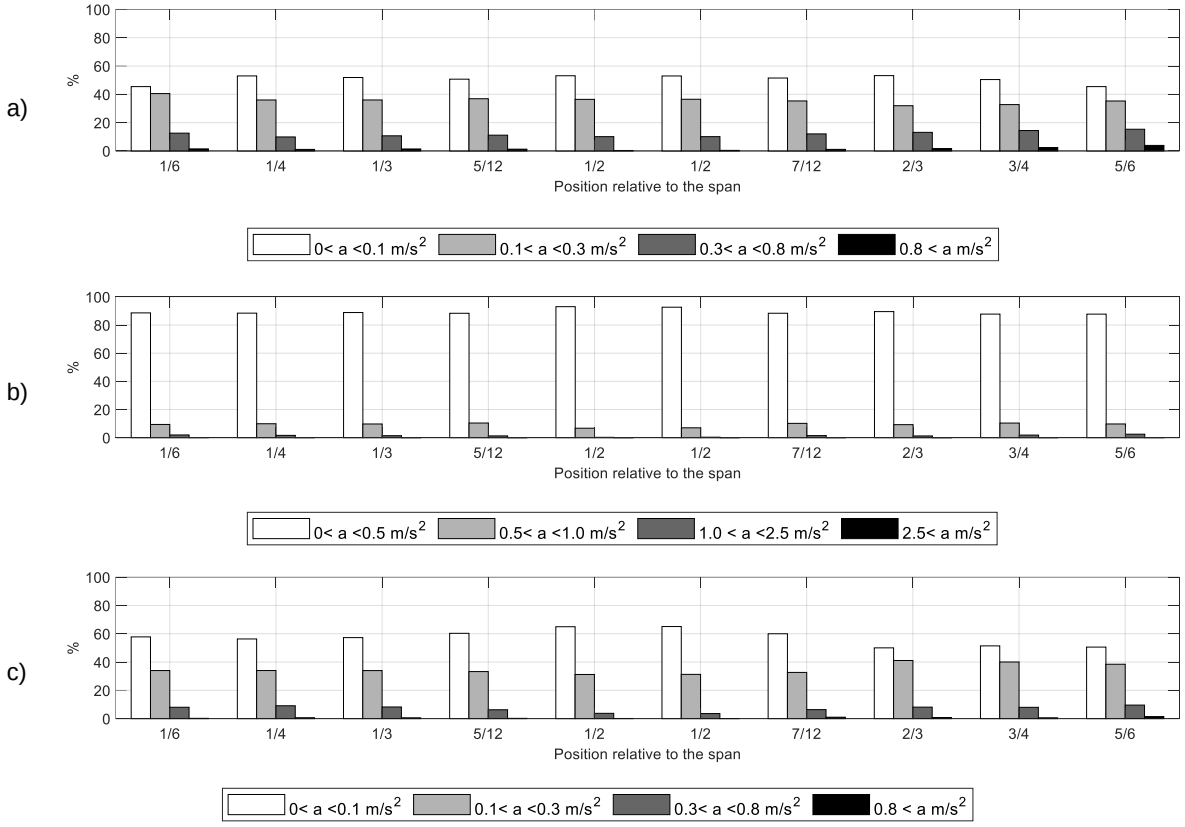

Figure S.1: Acceleration ranges and percentages for all monitoring positions, obtained during Test 2: a) X axis (longitudinal direction); b) Y axis (vertical direction); c) Z axis (lateral direction).

1

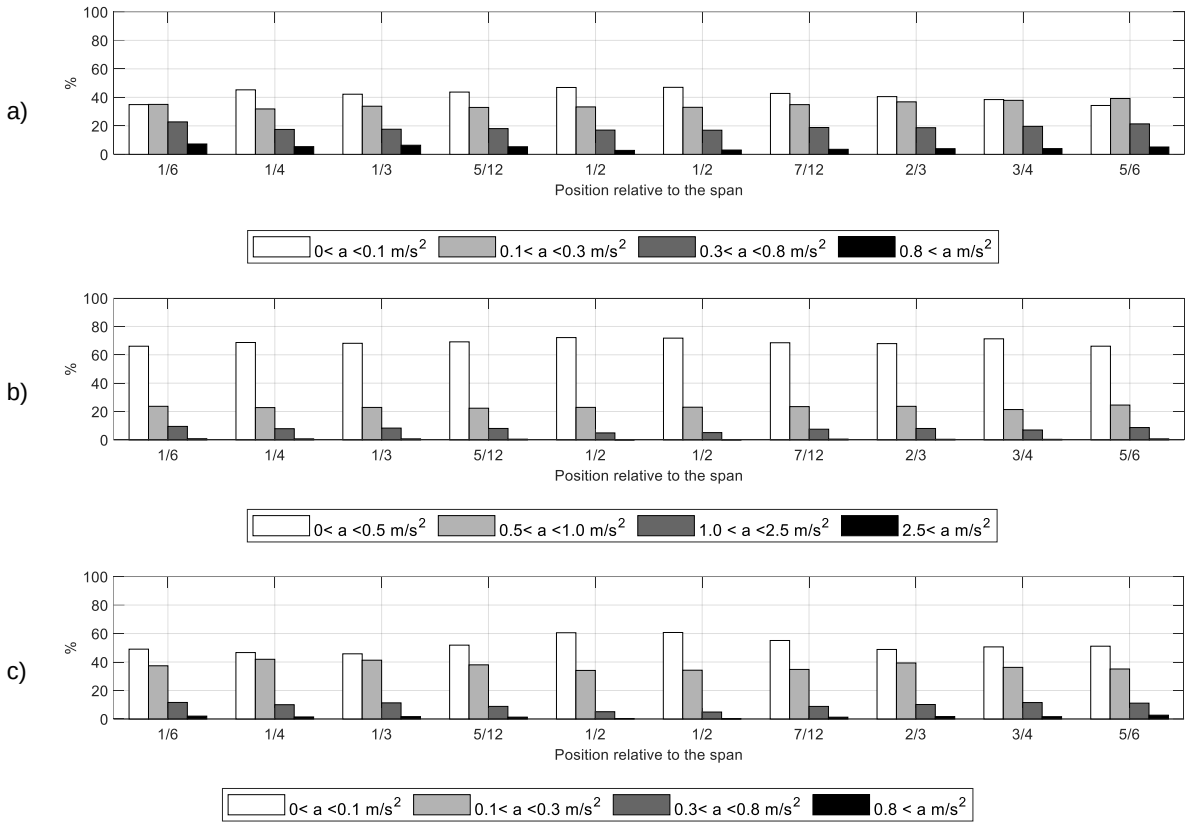

2 Figure S.2: Acceleration ranges and percentages for all monitoring positions, obtained during Test 3: a) X axis

3 (longitudinal direction); b) Y axis (vertical direction); c) Z axis (lateral direction).

4

1

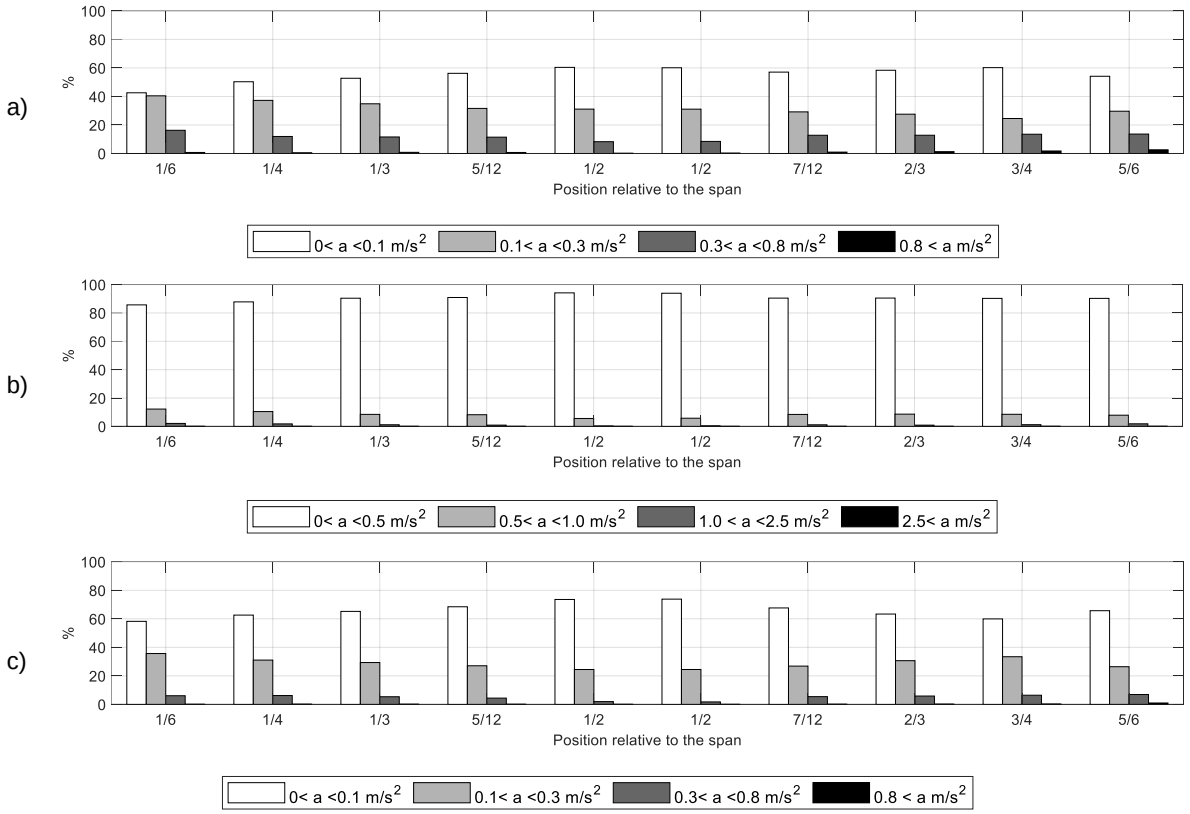

2 Figure S.3: Acceleration ranges and percentages for all monitoring positions, obtained during Test 4: a) X axis

3 (longitudinal direction); b) Y axis (vertical direction); c) Z axis (lateral direction).

4

Survey questions

Personal data:

1- Age:

2- Height:

3- Weight:

4- Nationality:

5- Did you feel fear before crossing the bridge?

Options: Yes/No

6- What was your comfort level regarding vibration when crossing the bridge?

Options: Maximum (practically imperceptible vibration) / Medium (merely perceptible vibration but not unpleasant) / Minimum (perceived vibration but not intolerable) / Unacceptable (intolerable)

7- Did you feel safe?

Options: Yes/No

8- Did you consider that too many people were on the bridge?

Options: Yes/No

9- Would you recommend the experience?

Options: Yes/No

10- Did the experience of crossing the bridge exceed your expectations?

Options: Yes/No